

UNCLASSIFIED

AD 401 699

*Reproduced
by the*

DEFENSE DOCUMENTATION CENTER

FOR

SCIENTIFIC AND TECHNICAL INFORMATION

CAMERON STATION, ALEXANDRIA, VIRGINIA



UNCLASSIFIED

NOTICE: When government or other drawings, specifications or other data are used for any purpose other than in connection with a definitely related government procurement operation, the U. S. Government thereby incurs no responsibility, nor any obligation whatsoever; and the fact that the Government may have formulated, furnished, or in any way supplied the said drawings, specifications, or other data is not to be regarded by implication or otherwise as in any manner licensing the holder or any other person or corporation, or conveying any rights or permission to manufacture, use or sell any patented invention that may in any way be related thereto.

401 699

SECOND QUARTERLY TECHNICAL PROGRESS REPORT
on

LARGE AREA THIN FILM CADMIUM SULFIDE
SOLAR CELL ARRAY INVESTIGATION
by

THE HARSHAW CHEMICAL COMPANY

SECOND QUARTERLY TECHNICAL PROGRESS REPORT

on

LARGE AREA THIN FILM CADMIUM SULFIDE
SOLAR CELL ARRAY INVESTIGATION

J. C. Schaefer
G. A. Wolff
E. R. Hill

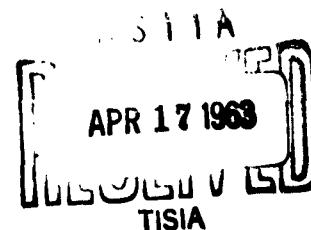
Solid State Research Laboratory
Crystal-Solid State Division
The Harshaw Chemical Company
1945 E. 97th Street
Cleveland 15, Ohio

Period of 15 December 1962 to 15 March 1963

21 March 1963

Contract No. AF 33(657)-9975
Project No. 8173, Task No. 817301

Flight Accessories Laboratory
Aeronautical Systems Division
Air Force Systems Command
United States Air Force
Wright-Patterson Air Force Base, Ohio



N O T I C E S

When Government drawings, specifications, or other data are used for any purpose other than in connection with a definitely related Government procurement operation, the United States Government thereby incurs no responsibility nor any obligation whatsoever; and the fact that the Government may have formulated, furnished, or in any manner licensing the holder or any person or corporation, or conveying any rights or permission to manufacture, use of sell any patented invention that may in any way be related thereto.

The information furnished herewith is made available for study upon the understanding that the Government's proprietary interests in and relating thereto shall not be impaired. It is desired that the Staff Judge Advocate (RDJ), Air Research and Development Command, Post Office Box 1395, Baltimore 3, Maryland, be promptly notified of any apparent conflict between the Government's proprietary interests and those of others.

FOREWORD

This report was prepared by The Harshaw Chemical Company, Solid State Research Laboratory, covering the work accomplished during the period from December 15, 1962, to March 15, 1963, under Contract AF 33(657)-9975. This report is being published and distributed prior to Air Force review. Its publication is for the exchange and stimulation of ideas and does not constitute approval by the Air Force of the findings or conclusion contained therein.

The work of this project deals with certain specific problem areas of the cadmium sulfide thin film front wall solar cell. Related contracts sponsored by the Air Force, by other Department of Defense Agencies, and by NASA at Harshaw and at other organizations are concerned with other aspects of cadmium sulfide solar cells, other photovoltaic conversion systems and with the investigation of the properties of various semiconductive materials with photovoltaic possibilities.

The detailed work of the project has been divided into three major parts with a principal investigator in charge of each. Cell Development efforts have been under the supervision of J. C. Schaefer and include the work on the orbital evaluation program, cell contacting, cell stability studies, cell and array construction, and other methods of film formation. Mr. Schaefer has been assisted in this area by R. J. Humrick, W. W. Baldauf, T. A. Griffin, and R. W. Olmsted. Materials Research, including materials purification and film structure studies, has been under the supervision of G. A. Wolff, who has been assisted by R. F. Belt and D. D. Bell in the former area and by J. R. Hietanen in the latter area. Cell Research efforts on basic barrier studies has been carried out by E. R. Hill. Technical and administrative direction of the project has been carried out by F. A. Shirland.

TABLE OF CONTENTS

	<u>Page</u>
INTRODUCTION AND SUMMARY.	1
PART I - CELL DEVELOPMENT	2
Orbital Evaluation	2
Panel Performance Characteristics.	2
Vibration Tests.	16
Cell and Array Construction.	23
Encapsulation Materials.	23
Pilot Line	24
Cell Contacting.	25
Cell Stability	26
Other Methods of Film Formation.	26
 PART II - MATERIALS RESEARCH.	 30
Purification of Cadmium Sulfide.	30
Film Structure Studies	32
Pole Figures of CdS Films on Glass and Molybdenum.	37
 PART III - BASIC BARRIER STUDIES.	 40
 WORK PLANNED FOR NEXT QUARTER	 48
 REFERENCES.	 50
 APPENDIX	

LIST OF TABLES

<u>Table</u>	<u>Title</u>	<u>Page</u>
I	Summary of Output Data.	3
II	Recommended Load Resistors for Orbital Panels	15
III	Simusoidal Vibration Test Data.	18
IV	Random Vibration Test Data.	23
V	Data on Lucite Encapsulated Cell.	24
VI	Cell and Array Data	25
VII	Effectiveness of Grid Materials	26
VIII	Electrophoretic Deposition Data	28
IX	Heat Treatment of Electrophoretic Deposits.	29
X	Zone Refined CdS Analysis	31
XI	Mass Spectrographic Analysis of CdS	32
XII	Etchants for CdS.	35

LIST OF FIGURES

<u>Figure</u>	<u>Title</u>	<u>Page</u>
1	I-V Characteristic Curves Orbital Panel 1.	4
2	I-V Characteristic Curves Orbital Panel 2.	5
3	I-V Characteristic Curves Orbital Panel 3.	6
4	I-V Characteristic Curves Orbital Panel 4.	7
5	I-V Curves vs. Temperature for Panel 1.	9
6	Power and Efficiency vs. Temperature for Panel 1.	10
7	Calibration Curves for Thermistors, Panel 1	11
8	Calibration Curves for Thermistors, Panel 2	12
9	Calibration Curves for Thermistors, Panel 3	13
10	Calibration Curves for Thermistors, Panel 4	14
11	Array Output vs. Angle of Incidence	17
12a	I-V Curve Before and After Sinusoidal Vibration Test (low-freq.).	19
12b	I-V Curve Before and After Sinusoidal Vibration Test (high-freq.)	20
12c	I-V Curve Before and After Sinusoidal Vibration Test in Parallel to Cell Plane	21
13	I-V Curves Before and After Random Vibration Test	22
14	Kronig-Penney Model No. 1	36
15	Kronig-Penney Model No. 2	37
16	Pole Figure (00.2 Plane) Glass Substrate Side	38
17	Pole Figure (00.2 Plane) Surface Side	39
18	Pole Figure (00.2 Plane) Molybdenum Substrate Side.	41
19	Pole Figure (00.2 Plane) Surface Side	42
20	Front Wall Cell Integrated Response in Sea Level Sunlight Cell No. 700	44
21	Front Wall Cell Integrated Response in Extraterrestrial Sunlight Cell No. 700.	45
22	Front Wall Cell Integrated Response in Sea Level Sunlight Cell No. 339 MN.	46
23	Front Wall Cell Spectral Response, Cell No. 339 MN.	47

INTRODUCTION AND SUMMARY

This is the second quarterly progress report on Contract AF 33(657)-9975 concerned with the investigation of large area CdS film cells.

The effort for a large portion of this quarter has been directed toward the completion and testing of the four orbital test panels. The temperature, shock and acceleration tests were performed during the first quarter, while the sinusoidal and random or white noise vibration tests were conducted during this period. No detrimental cell effects were noted. The panels were tested under tungsten light and sunlight, and were found to have efficiencies of 2.4 to 2.9% with power to weight ratios of 9.2 to 12.5 watts per pound. Various graphs indicating expected performance in space are included.

Completion of this high priority effort permitted the emphasis to return to the research and development phases. Uniform coatings of CdS have been electrophoretically deposited on molybdenum substrates from nonaqueous solutions. New plastics and collector grid materials have been tested. Pole figure techniques are being applied to films deposited on various substrates to determine the effect of substrates on grain orientation. Studies of grain orientation have been continued using light-figure and x-ray diffraction techniques.

A paper given by Dr. G. A. Wolff and J. Hietanen at the International Symposium on Condensation & Evaporation of Solids, September, 1962, at the Dayton Biltmore Hotel, Dayton, Ohio, and sponsored by the Thermophysics Branch, Physics Laboratory, Directorate of Materials and Processes, Aeronautical Systems Division, Wright-Patterson Air Force Base, Ohio, has been included as an appendix because of its direct relationship to the research phases of this program.

PART I - CELL DEVELOPMENT

Orbital Evaluation

During this reporting period, the four solar cell orbital test panels, each consisting of 3-6" x 6" arrays were completed, tested, and delivered to the contract monitor on schedule.

For the preparation of these panels an attempt was made to match the individual 3" x 3" cells in groups of four according to their maximum power values which were then laminated together as 6" x 6" arrays. The arrays were matched according to their values of current-at-maximum-power. Every third array also contained two heat sensors for the purpose of monitoring the surface temperatures. Table I summarizes the output data for these arrays and panels.

Panel Performance Characteristics

Figures 1, 2, 3, and 4, represent the I-V characteristic curves for Panels 1, 2, 3, and 4, respectively. In each case, the solid curve, labelled (1), is the actual data curve taken in tungsten light equivalent to 100 mw/cm² terrestrial sunlight. The curve labelled (2), in each case represents an extrapolation of the data of curve (1) to the higher intensity (140 mw/cm²) of extra terrestrial sunlight, but with no provision for the change in spectral distribution. A quantitative prediction of the effect of the change in spectral distribution in outer space is not known though it is believed that it will increase somewhat the output of CdS front wall cells over what has been calculated here. Curve (2) has been constructed on the basis of the known effect (separately measured on representative arrays of cells) of increasing light intensity on the I-V characteristics, from open circuit to short circuit condition. From 100 to 140 mw/cm² sunlight intensity, the OCV increases slightly, about 1%, while the SCC increases linearly by 40%. There appears to be no pronounced change in the rectangularity of the characteristic curve.

The curve labelled (3) in Figures 1, 2, 3, and 4, represents the calculated effect of the increase in temperature which is expected to occur in space. Based on tests at the Chance-Vought Company facility at Dallas, Texas, last summer, and on independent tests in our laboratories, it is expected that the present design panels will reach a steady state temperature of 110°F in full sunlight in space outside the earth's atmosphere. An increase in operating temperature from 70°F. to 110°F. will (by separate measurements which are discussed in the following paragraph) be expected to result in a drop in the open circuit voltage of 5.1%, but an increase in the short circuit current of 9.7%. This results in these cases in an actual increase in the expected maximum power output. The maximum power rectangle has been constructed in each case for both the actual data curve (i.e., 100 mw/cm² at 70°F.) and for the expected space performance curve (i.e., 140 mw/cm² at 110°F.) and the corresponding load lines have been drawn.

Typical arrays of CdS front wall film cells, constructed at the same time as the orbital test panels, were carefully tested at selected temperatures

TABLE I

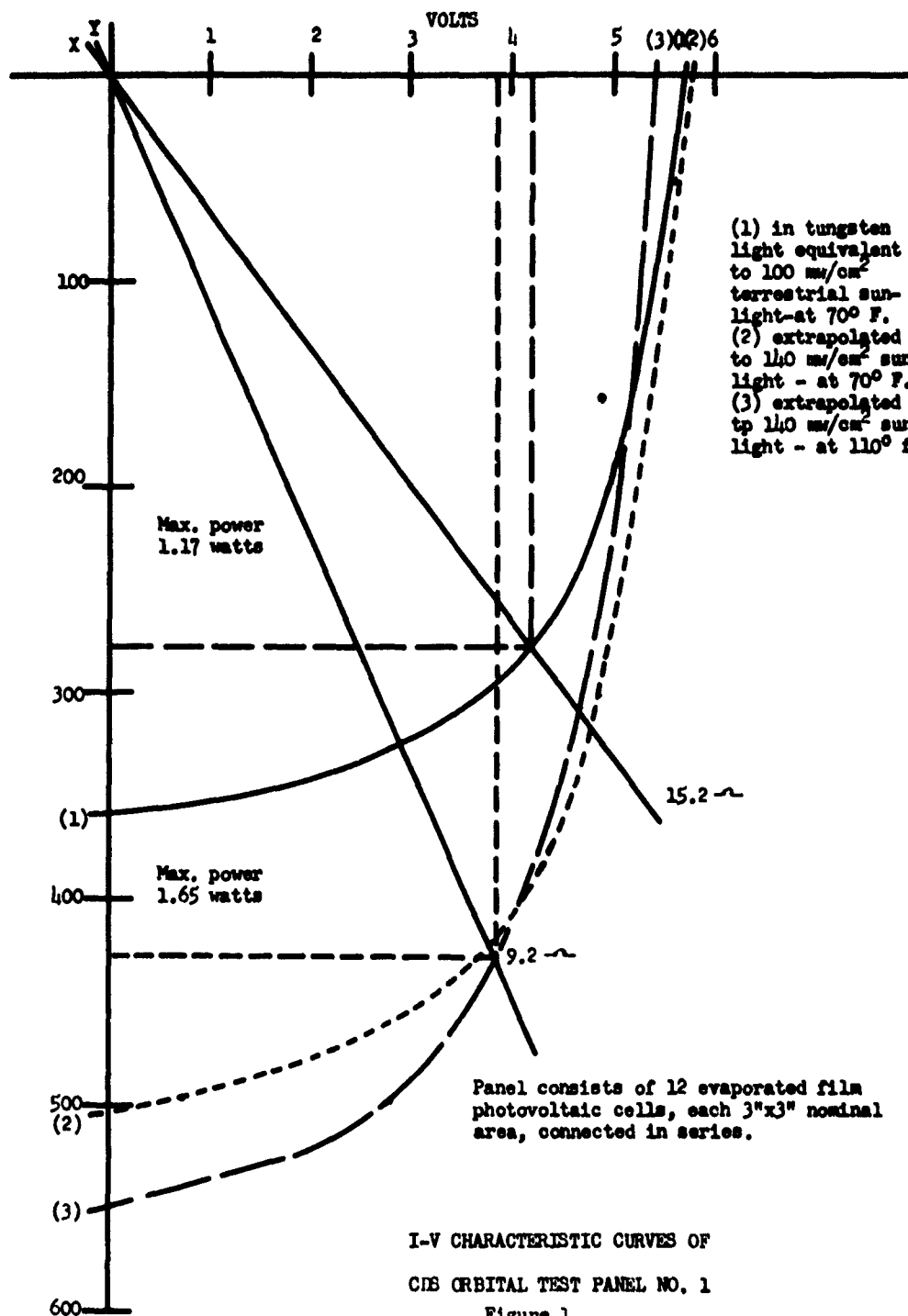
SUMMARY OF OUTPUT DATA

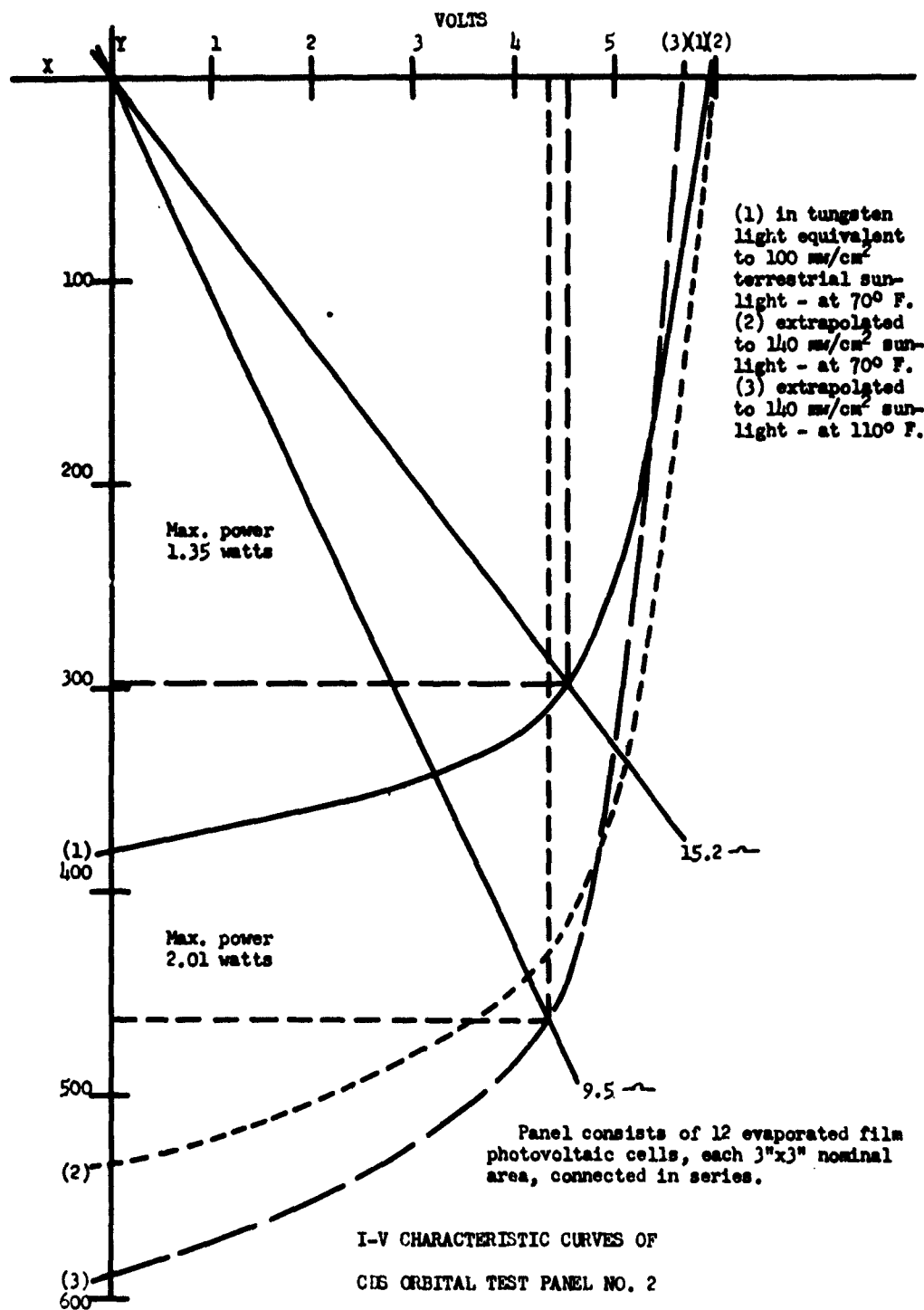
CdS Front Wall Film Solar Cell

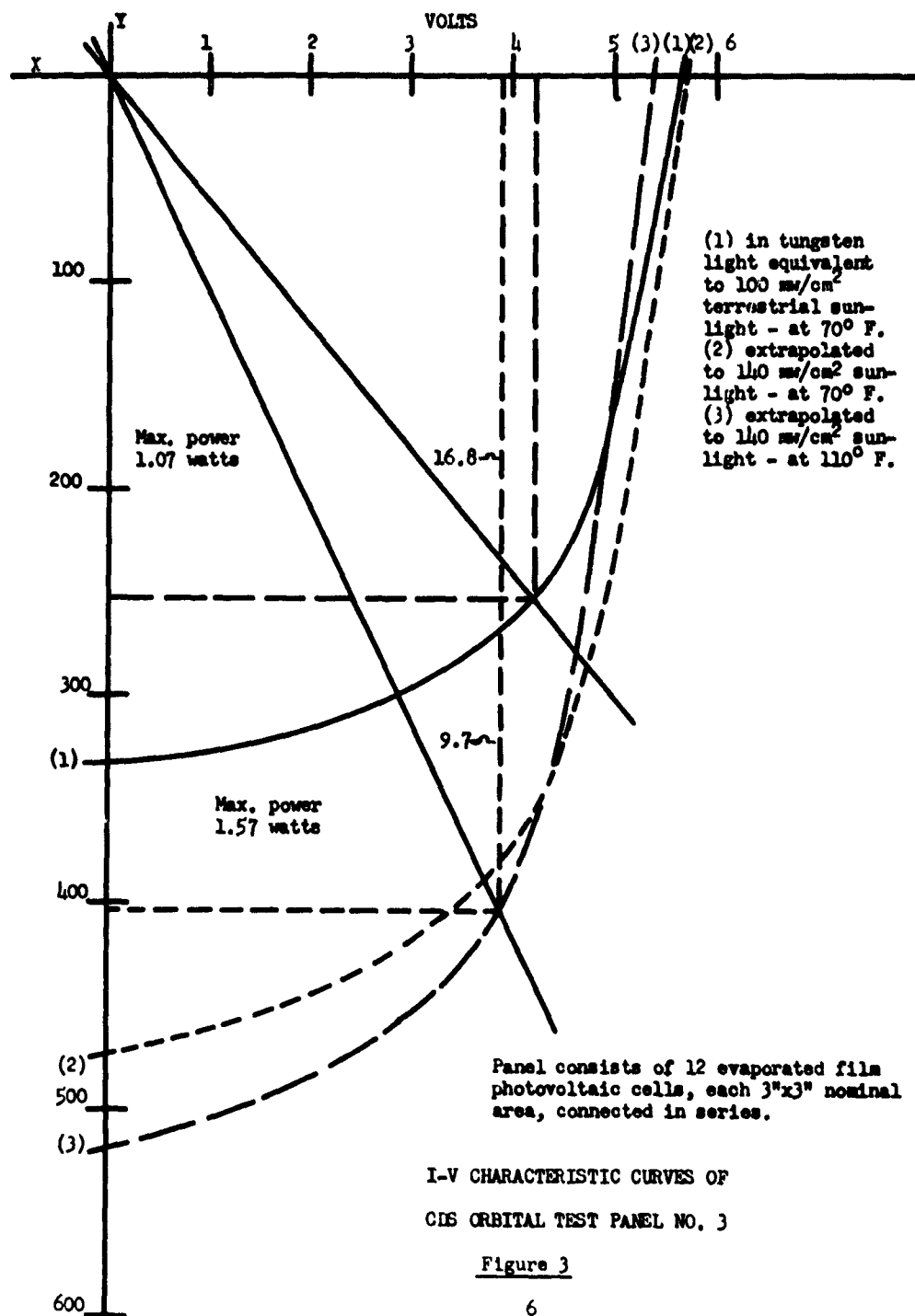
Arrays for Orbital Evaluation

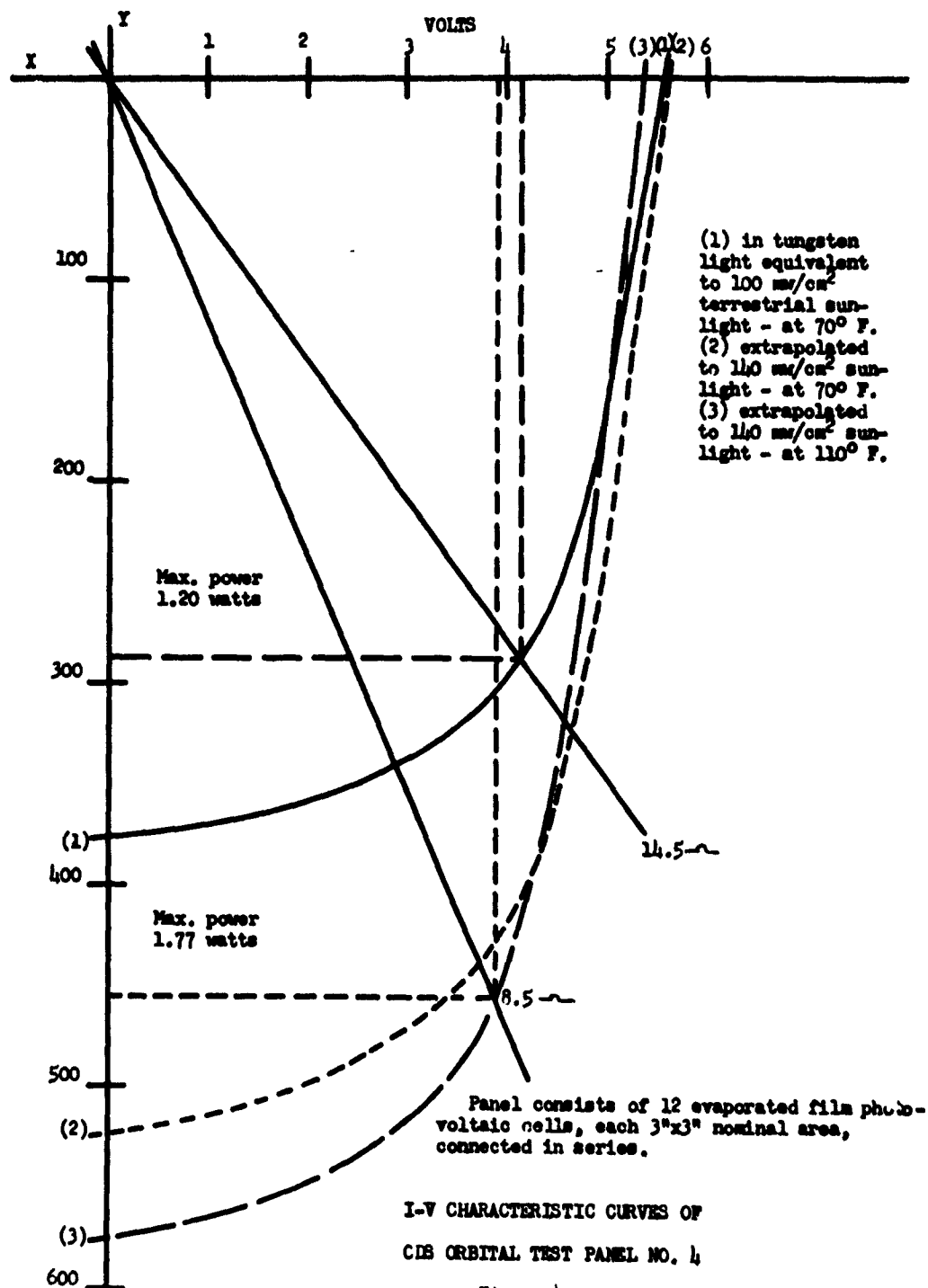
Terrestrial Conditions - 70°F. - 100 mw/cm²Space Conditions - 110°F - 140 mw/cm²

Panel	Array	Terrestrial Conditions - 70°F. - 100 mw/cm ²				Active Area (cm ²)	Space Conditions - 110°F - 140 mw/cm ²				Eff Watts/lb
		V _{oc}	I _{sc}	V _{mp}	I _{mp}		V _{oc}	I _{sc}	V _{mp}	I _{mp}	
		(volts)	(ma)	(volts)	(ma)		(volts)	(ma)	(volts)	(ma)	(watts) %
1	340	2.0	340	1.6	275	450.					
	342	2.0	340	1.5	290						
	353*	1.8	325	1.2	265						
	Total	5.72	360	4.20	278		73.5	5.43	550	3.85	428 1.65 2.6 10.2
2	354	2.0	330	1.5	270	458.					
	341	2.0	305	1.5	270						
	351*	2.0	310	1.5	260						
	Total	5.90	380	4.5	298		73.2	5.68	590	4.35	462 2.01 3.1 12.5
3	350	1.9	350	1.2	270	455.					
	348	2.0	290	1.5	250						
	357*	2.0	300	1.5	240						
	Total	5.6	318	4.23	252		77.1	5.40	520	3.90	403 1.57 2.5 9.2
4	335	1.9	360	1.4	300	448.					
	336	2.0	330	1.5	260						
	352*	2.0	290	1.5	240						
	Total	5.8	375	4.15	288		71.6	5.38	575	3.90	455 1.77 2.8 11.2









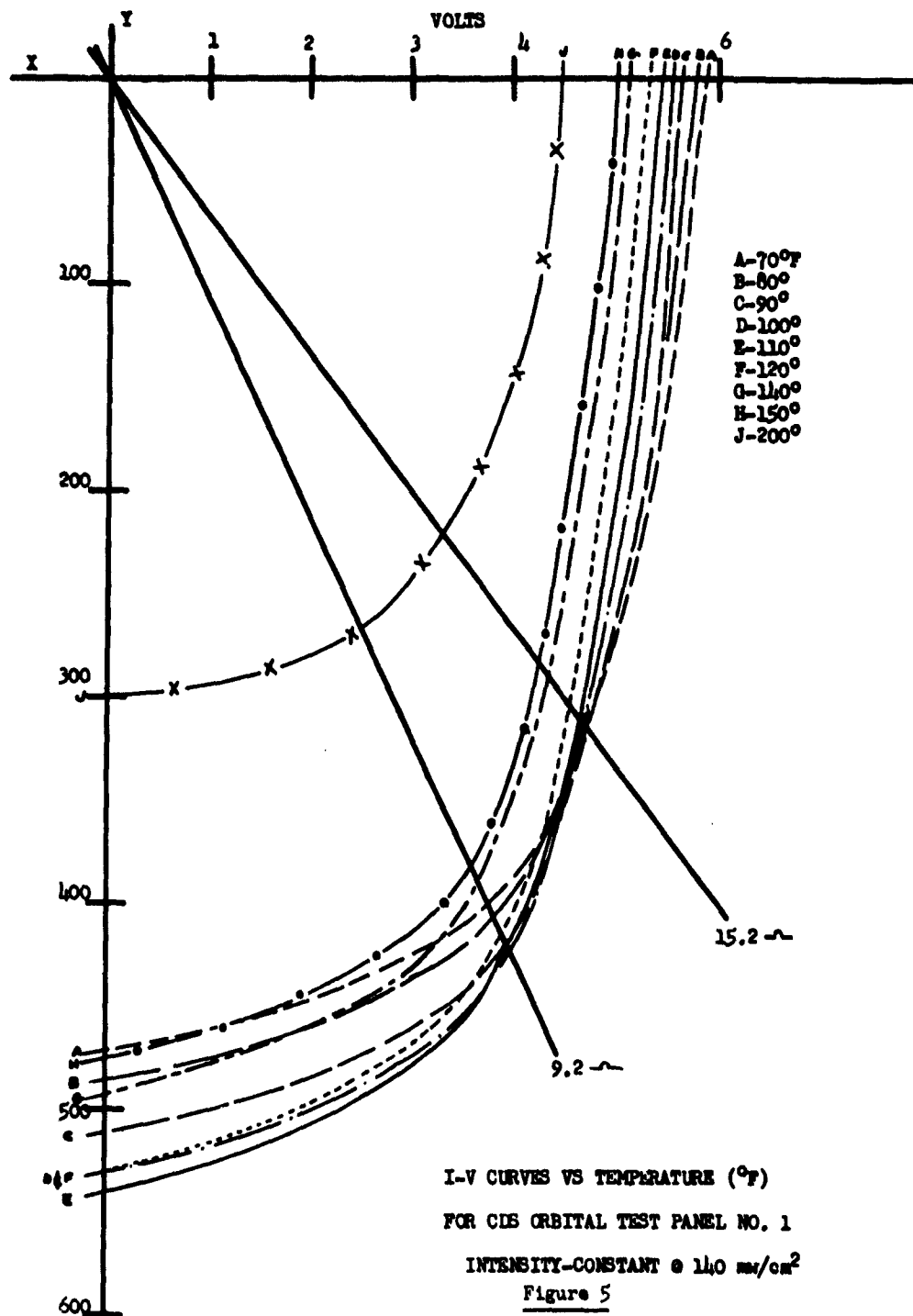
(1) in tungsten light equivalent to 100 mw/cm² terrestrial sunlight - at 70° F.
(2) extrapolated to 140 mw/cm² sunlight - at 70° F.
(3) extrapolated to 140 mw/cm² sunlight - at 110° F.

between the extremes of -40° and $+200^{\circ}\text{F}$. I-V characteristic curves were taken at each temperature. The proportionate change in current at various percentages of open circuit voltage was established for each temperature and used to calculate the expected effect of temperature on the output of each of the 4 orbital test panels. Figure 5 shows the calculated I-V curves for Panel No. 1 at selected temperatures between 70°F and 200°F . As can be seen, the open circuit voltage drops steadily with increasing temperature. However, the short circuit current increases with increasing temperature and reaches a maximum at 110°F . At higher temperatures the current decreases. The result of this is that the I-V characteristic curves cross each other.

Two load lines are entered on Figure 5. The load line of 15.2 ohms (which is the load for maximum power transfer for this panel at 70°F and 100 mw/cm² sunlight) would show a steady drop in power output with increasing temperature. However, the load line of 9.2 ohms (which is the load for maximum power transfer for this panel at 110°F and 140 mw/cm² sunlight) reveals a different pattern because of its steeper slope. It intersects the I-V curves mostly after their cross overs. Figure 6 plots the expected power (and conversion efficiency) for this panel in extraterrestrial sunlight with a fixed load of 9.2 ohms, over the complete temperature range of -40 to $+200^{\circ}\text{F}$. It is evident from this curve that the expected operating temperature of 110°F . in space is indeed fortunate.

Figures 7, 8, 9, and 10, give the calibration curves of the thermistors that were encapsulated in panel number 1, 2, 3, and 4, respectively. In each case, the manufacturers calibration has been given along with the calibration taken in our own laboratory. It is seen that there is close agreement in all but one instance. In order to prevent possible confusion between the two thermistors that were encapsulated in each panel (one at the front surface of the cells, and one at the back surface) the thermistors were selected so that in each case the temperature versus resistance curve over the entire range was identical for both thermistors. Hence, only one calibration curve is presented for each panel.

Table II includes the recommendations for the load resistances for these orbital evaluation panels. Following the apparent requirements of the telemetry, the load resistances for each panel for the conditions of open circuit, short circuit, and maximum power transfer have been indicated. Resistance R_1 and R_2 in the table represent in summation the total recommended resistance for the external load, while R_2 represents that portion of the total resistance across which the voltage measuring equipment would be connected. Following the earlier indications from the vehicle contractor, the resistances have been so selected as to give readily measurable voltage drops at the meter. For short circuit conditions the resistance has been calculated to provide an arbitrary expected voltage reading of 1 volt. As can be seen from Figures 1, 2, 3, and 4, this will produce a slight error in the calculated value of the short circuit current due to the lack of rectangularity of the I-V characteristic. The value of R_1 is zero for both short circuit and maximum power conditions for all 4 panels. For open circuit conditions the voltage has been divided so that the capacity of the meter will not be exceeded. In so doing an allowance has been made for a safety factor of about 10% of full scale, just in case the cells should perform much better than expected.



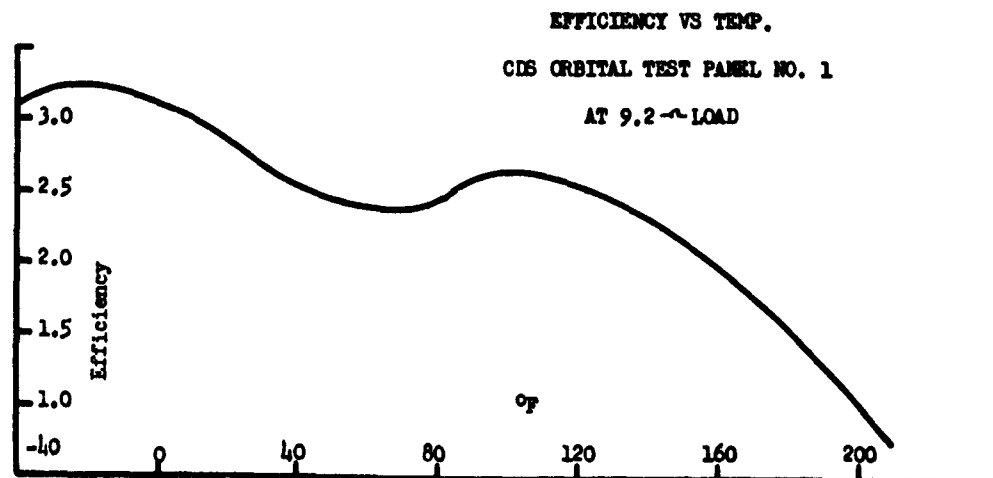
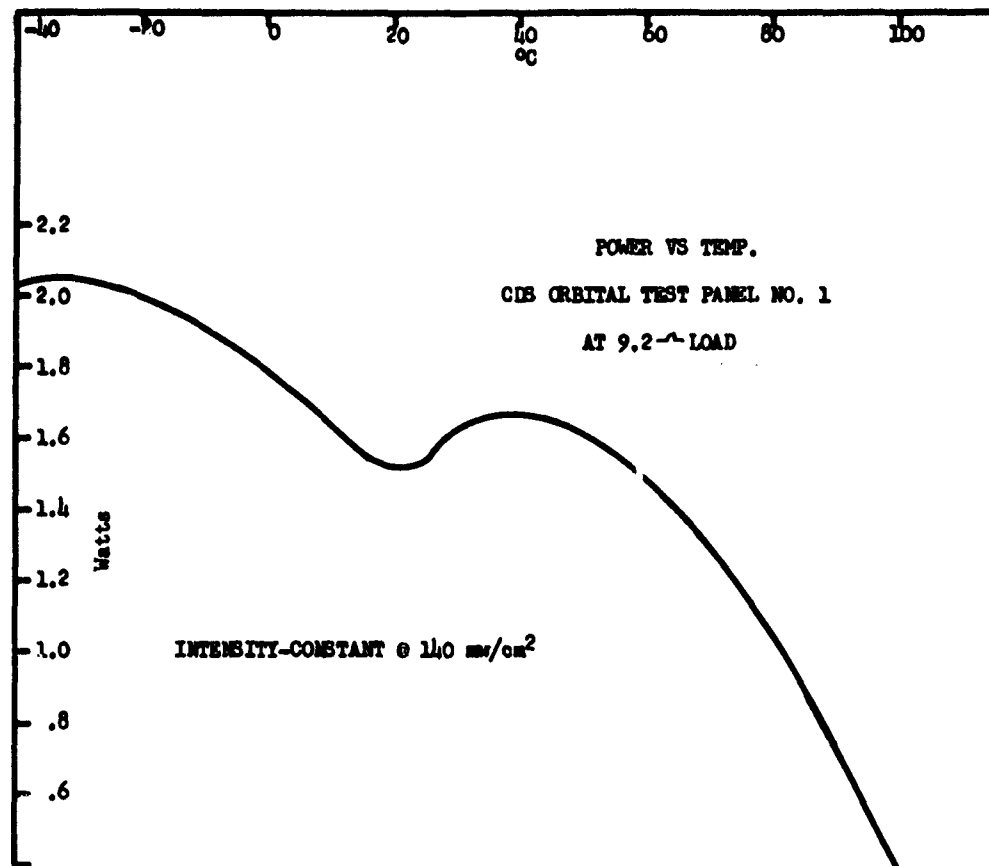


Figure 6

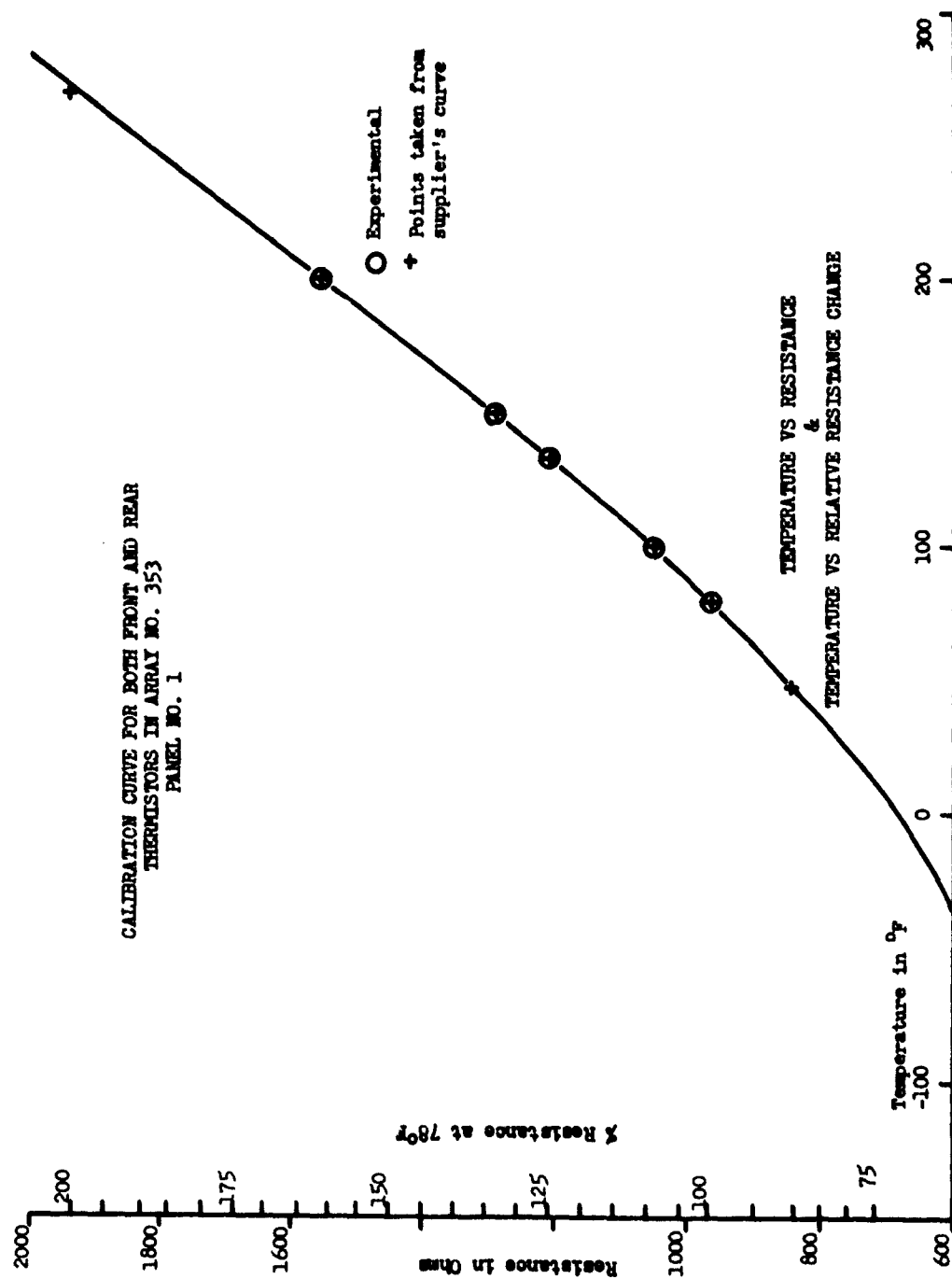


Figure 7

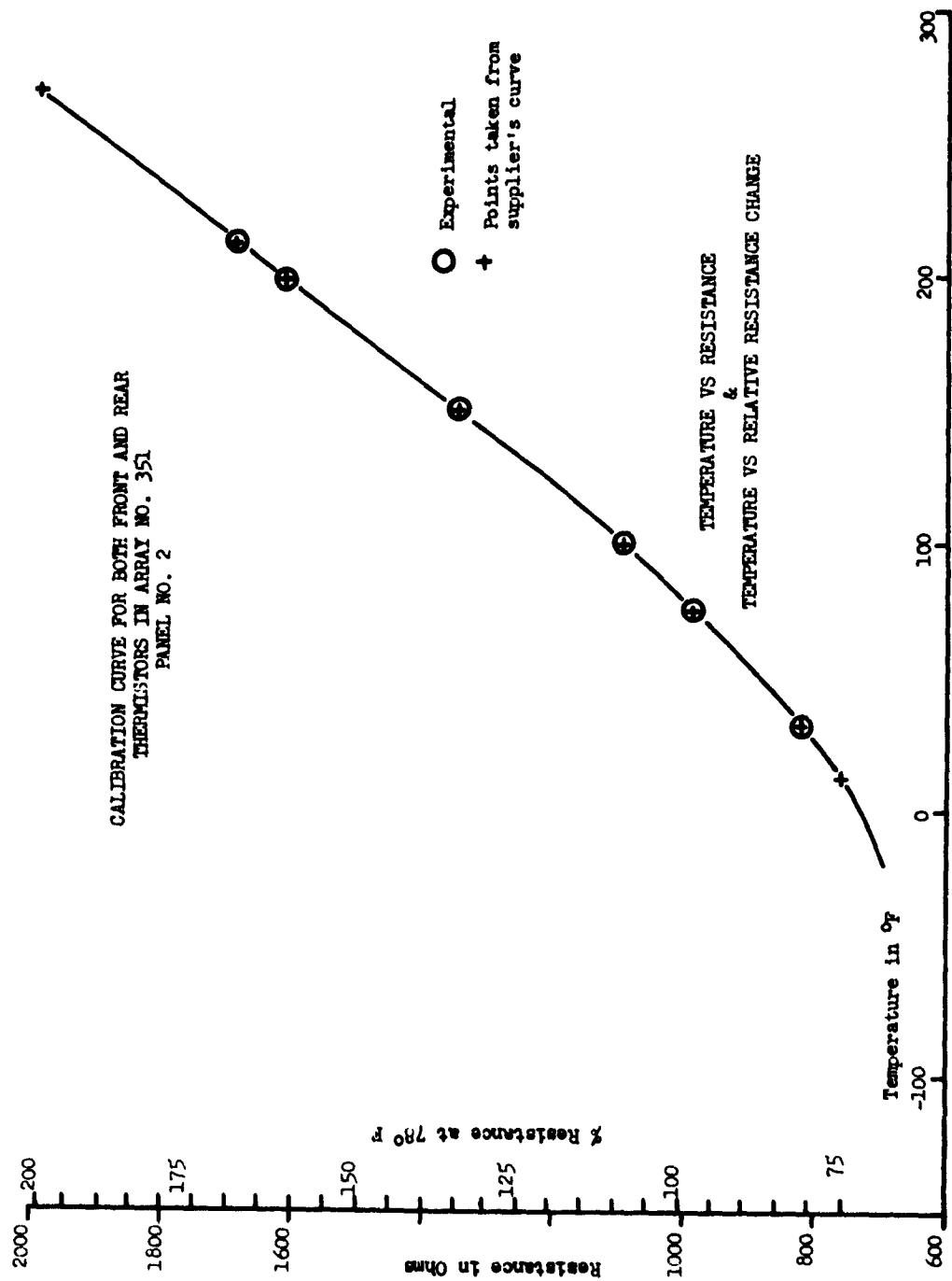


Figure 8

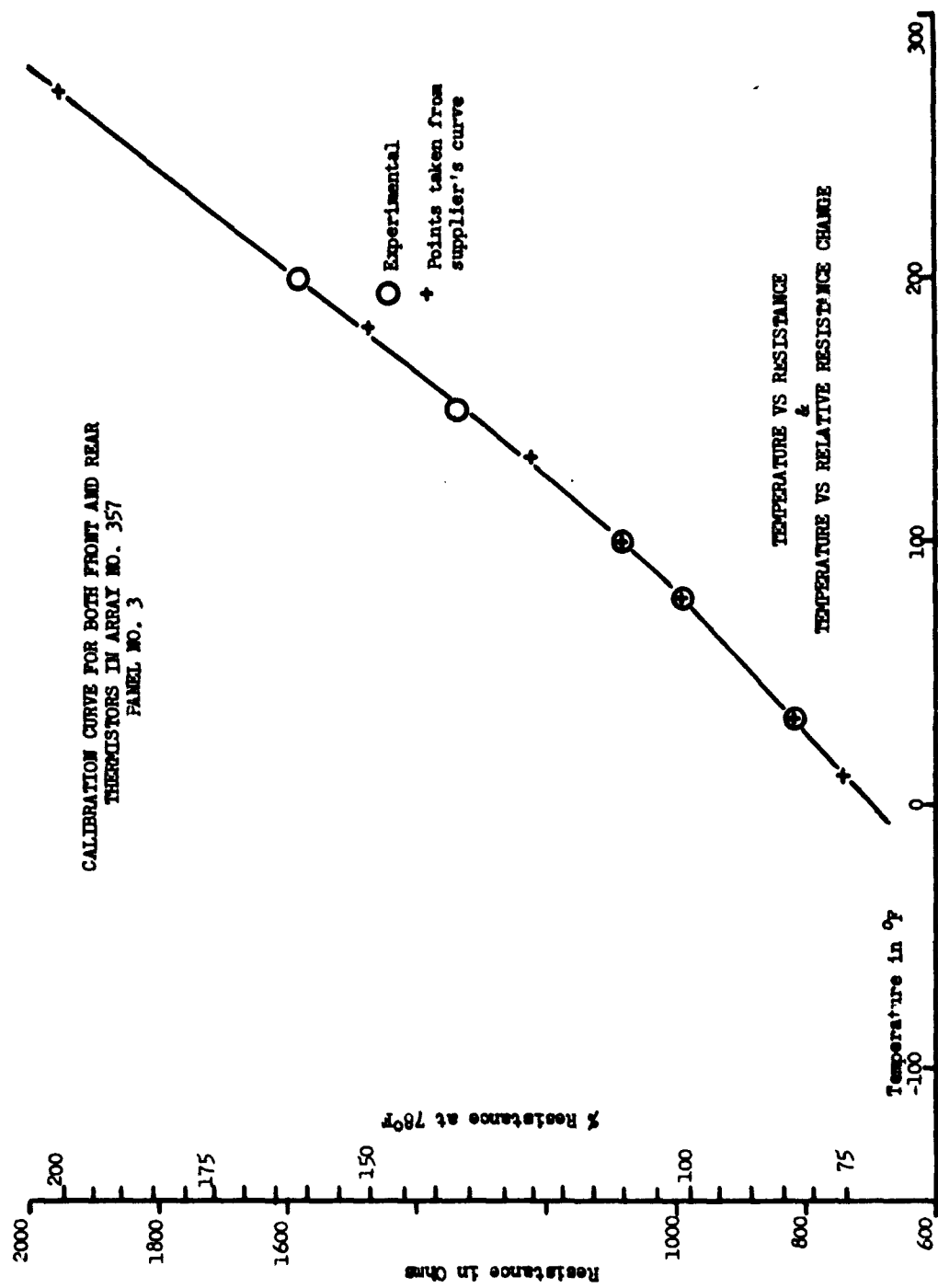


Figure 9

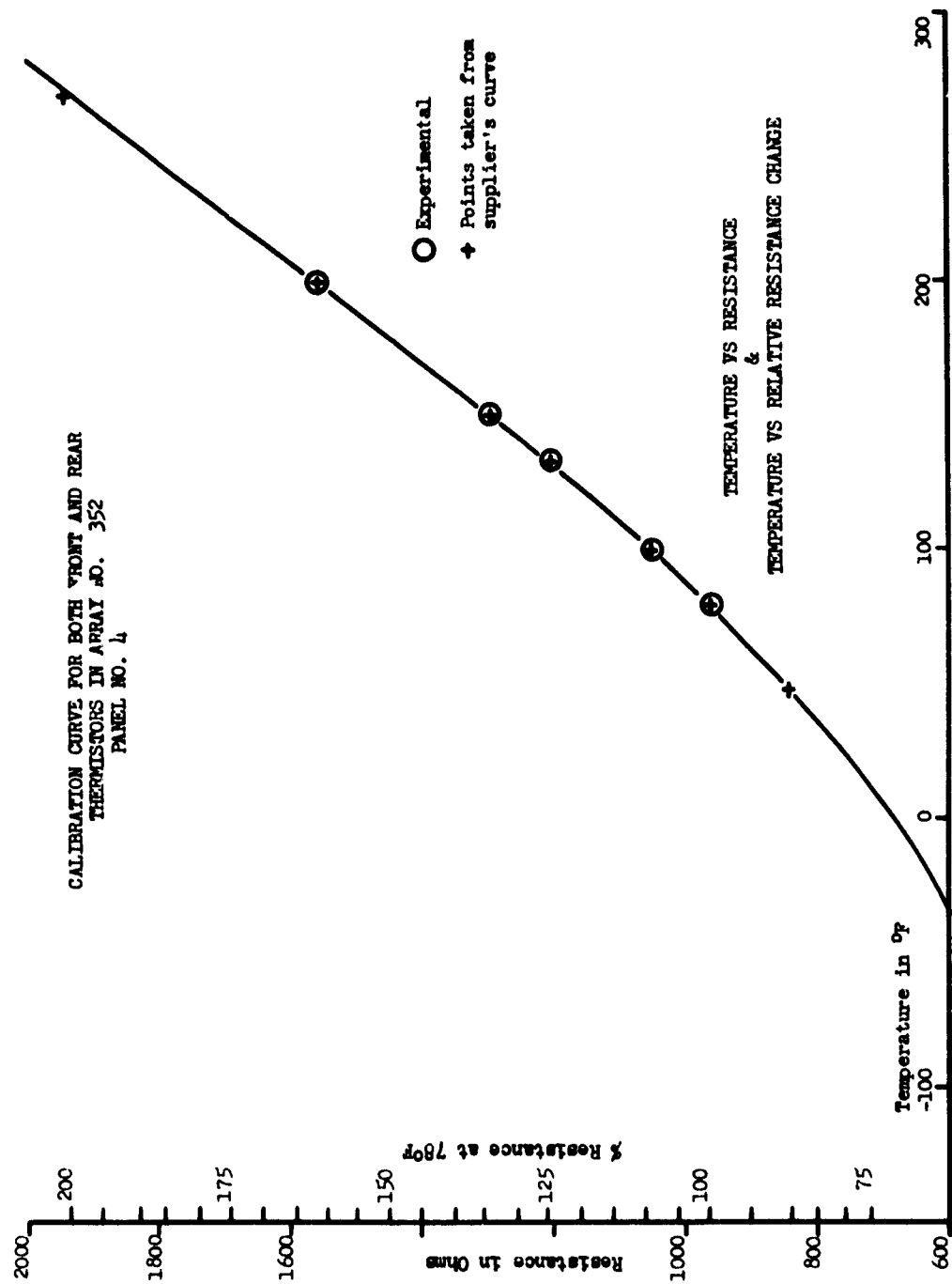
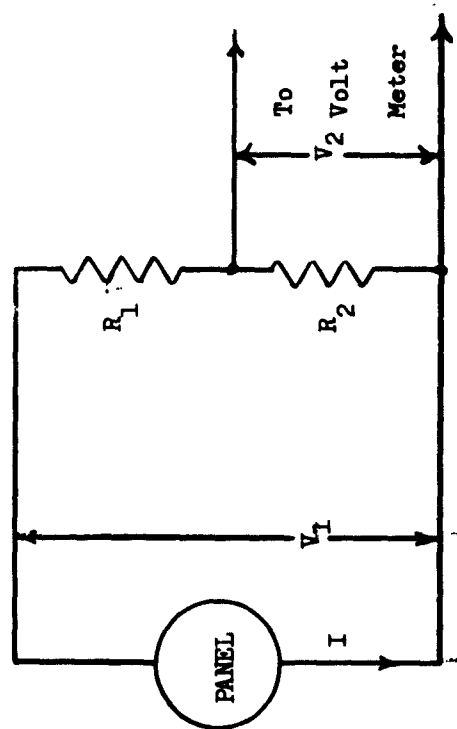


Figure 10

TABLE II
RECOMMENDED LOAD RESISTORS FOR ORBITAL EVALUATION OF CDS PANELS

<u>PARAMETER</u>	<u>PANEL NO. 1</u>		<u>M.P.</u>		<u>PANEL NO. 2</u>		<u>M.P.</u>		<u>PANEL NO. 3</u>		<u>M.P.</u>		<u>PANEL NO. 4</u>		<u>M.P.</u>
	<u>O.C.</u>	<u>S.C.</u>	<u>O.C.</u>	<u>S.C.</u>	<u>O.C.</u>	<u>S.C.</u>	<u>O.C.</u>	<u>S.C.</u>	<u>O.C.</u>	<u>S.C.</u>	<u>O.C.</u>	<u>S.C.</u>	<u>O.C.</u>	<u>S.C.</u>	
R ₁	170	0	0	0	170	0	0	0	170	0	0	0	170	0	0
R ₂	830	1.87	9.20	830	1.75	9.50	830	1.98	9.70	830	1.77	8.50			
V ₁	5.48	1.0	3.85	5.65	1.0	4.35	5.40	1.0	3.90	5.35	1.0	3.90			
V ₂	4.55	1.0	3.85	4.69	1.0	4.35	4.48	1.0	3.90	4.43	1.0	3.90			
I	5	535	420	6	570	460	5	505	405	5	565	460			



R_1 & R_2 in ohms

V_1 = Voltage Generated across Panels

Calculated as $V_1 = (R_1 + R_2) \sqrt{V_2/R_2}$
(including 0.46 ohm Lead Wires)

V_2 = Voltage read at Meter

The values given above are values that are expected to be read under the conditions fo O.C., S.C. and maximum Power.

$I = \text{Current flowing out of panel calculated as } I = V \frac{2}{R_2}$
(given in ma)

There is one source of constant error in all of the above calculations and in the I-V characteristic and temperature performance curves. This is the resistance of the lead wires. Each array of each panel has 2 lead wires of 28 gage polyolefin insulated wires, as specified. Each of these leads is 24" long. The measurements of output of these arrays and panels have been made utilizing the leads, but without making any allowance for the resistance of the leads. The resistance of the leads as they were connected for test purposes totalled 0.46 ohms. Thus the actual output of the panels must in each case be slightly better than indicated by the curves presented here. When the arrays are actually mounted on the orbital test boom, a measure must be made of the total length of the leads that are in the series connection so that allowance can be made for the effect of the leads in interpreting the tele-metered data.

Figure 11 is a plot of the data obtained by varying the angle of incidence of a 6" x 6" array (No. 335MN) in sunlight. The array output was measured at 10 degree intervals from 0° to 90°. The array efficiency obtained normal to the sun was multiplied by the cosine of each angle and the resultant values are also plotted in Figure 11. It can be readily seen that the array efficiency follows the cosine law.

Vibration Tests

Additional vibration tests were performed during this report period, namely, sinusoidal and random or white noise. As in the previous tests, no appreciable damage effects were noted.

The sinusoidal vibration test consists of applying to each of three mutually perpendicular axes the following: 5-14 cps, 0.5 in. double amplitude; 14-40 cps., 5g; 40-400 cps, 7.5g; 400-3000 cps, 15g; at a constant rate in a single sweep in not less than 25 minutes. The test was performed at Lear-Siegler Corporation, Cleveland, Ohio, requiring, as in the previous acceleration and shock tests, the transportation of test equipment for the measurement of cell output. The test equipment has been previously reported⁽¹⁾. Measurements were made before and after each vibration test performed in each direction. No visual damage was noted at any time during the test and from the I-V data in Table III and plotted in Figures 12a, b, and c, it can be seen that no real change in array output took place. The test array No. 289MN, was the same one used for the acceleration and shock tests.

The final phase of the vibration test was conducted on the same array as on the preceeding tests i.e. No. 289MN and consisted of applying to each of the three mutually perpendicular axes vibrations of .05 g² per cycle per second from 15-2000 cps, for 5 minutes each. The test was performed at the Thompson-Ramo-Wooldrige, Rocky Mount, Virginia, testing laboratory. During this vibration materials was made and upon return to the Harshaw Laboratory, the array output was measured. No significant difference can be noted in the data in Table IV on the I-V curves plotted in Figure 13.

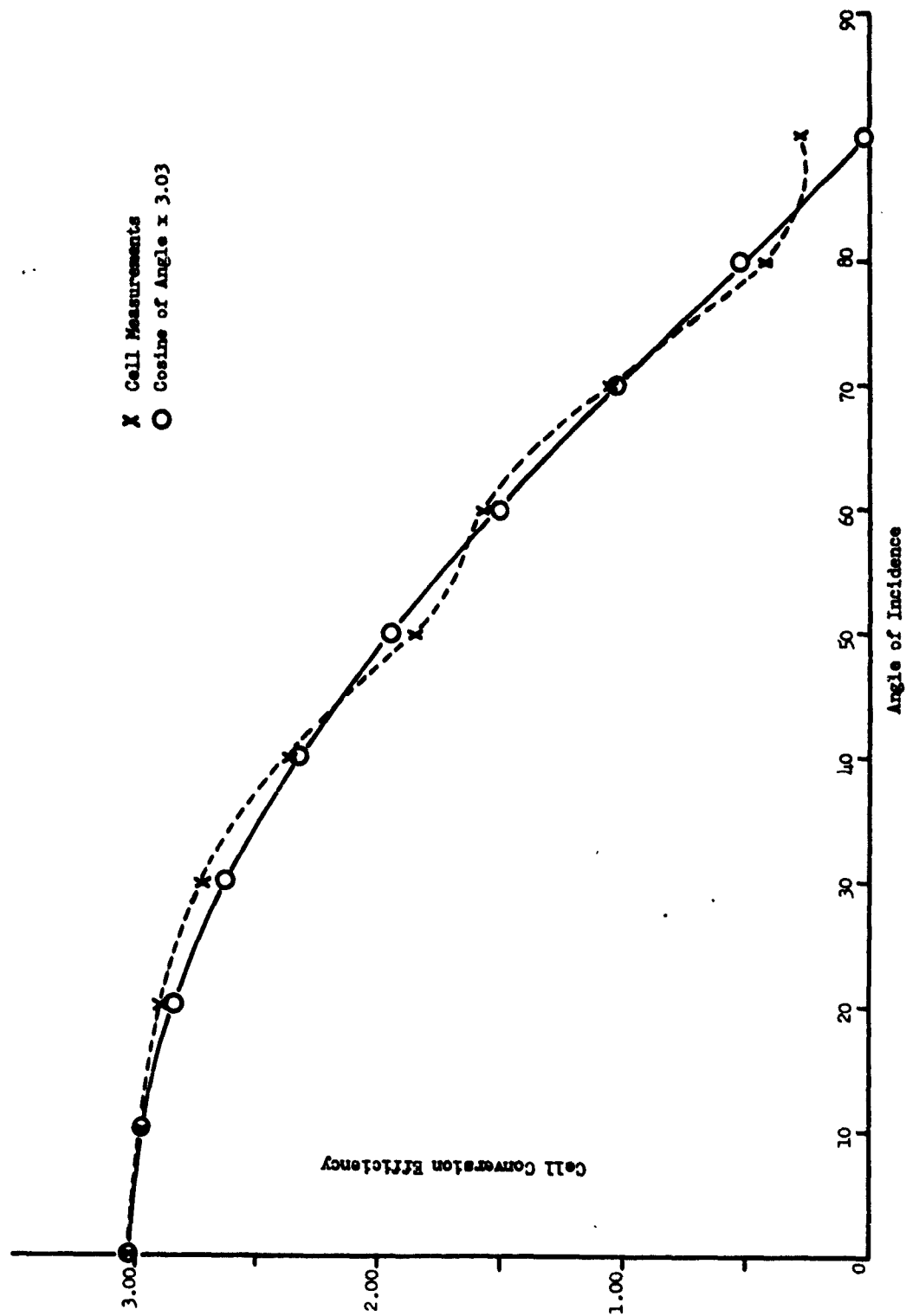
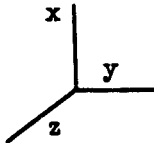


Figure 11

TABLE III

SINUSOIDAL VIBRATION TEST DATA

		<u>Time of Test</u>	<u>Load Resistance in Ohms</u>	<u>Voltage</u>	<u>Current in ma</u>
Array No. 289MN	Harshaw Chemical Solid State Lab.		-	2.1	0
			8.2	1.83	223
			5.0	1.47	294
			3.0	.97	324
			1.4	.49	350
	After Vibration in X-X axis		-	2.1	0
			8.2	1.80	220
			5.0	1.46	292
			3.0	.96	320
			1.4	.50	357
	After Vibration in Y-Y axis		-	2.1	0
			8.2	1.80	220
			5.0	1.43	286
			3.0	.93	310
			1.4	.47	336
	After Vibration in Z-Z axis		-	2.15	0
			8.2	1.81	221
			5.0	1.46	292
			3.0	.97	323
			1.4	.49	350

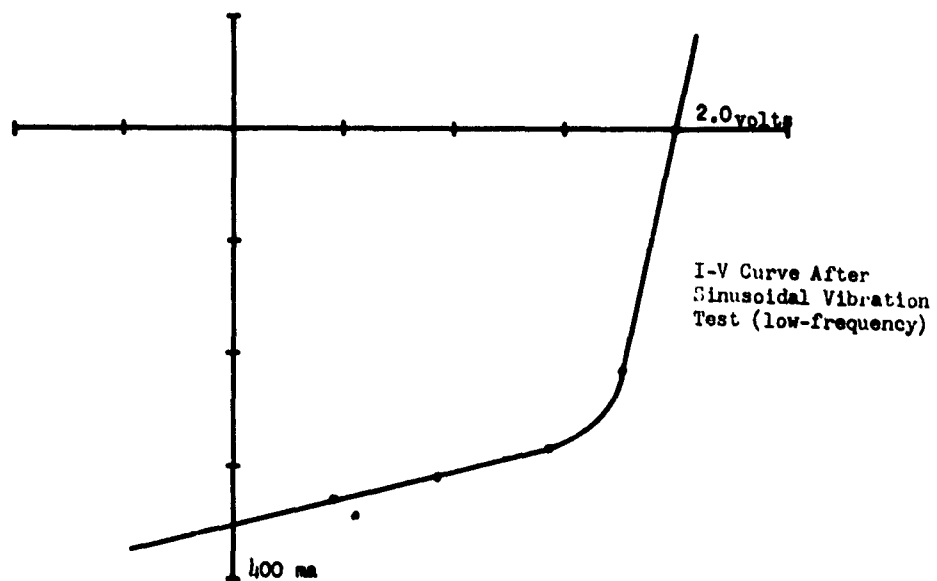
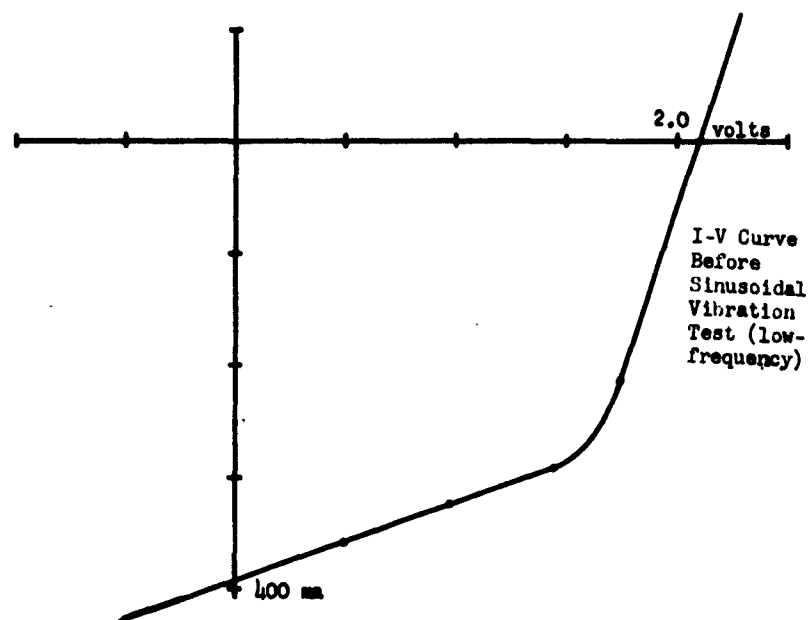


Figure 12a

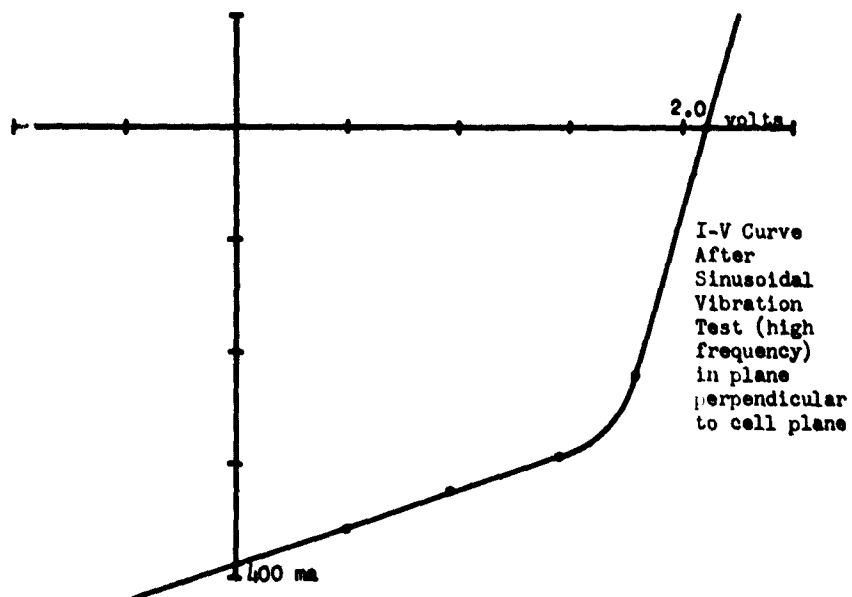
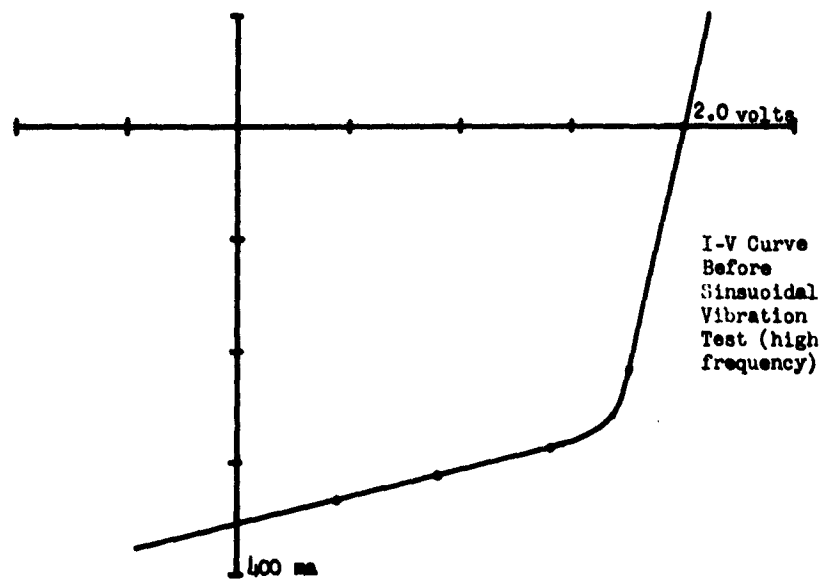


Figure 12b

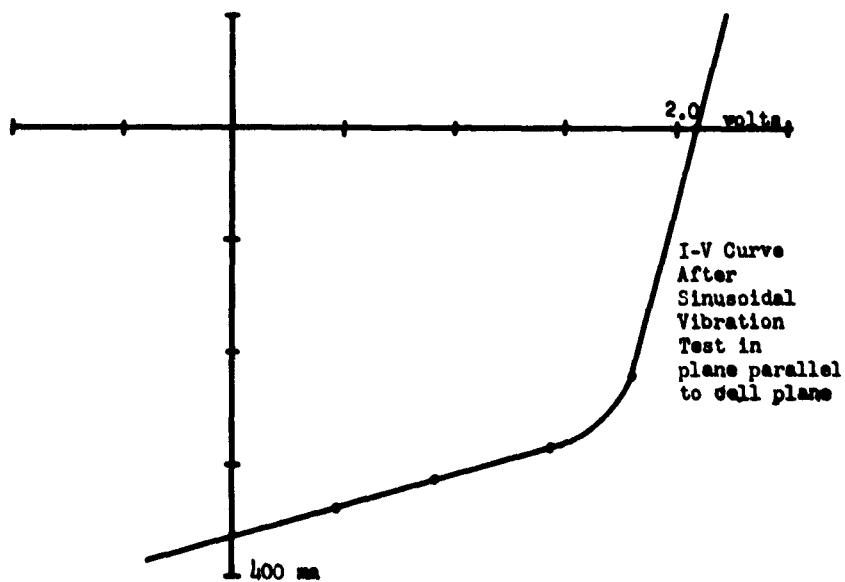
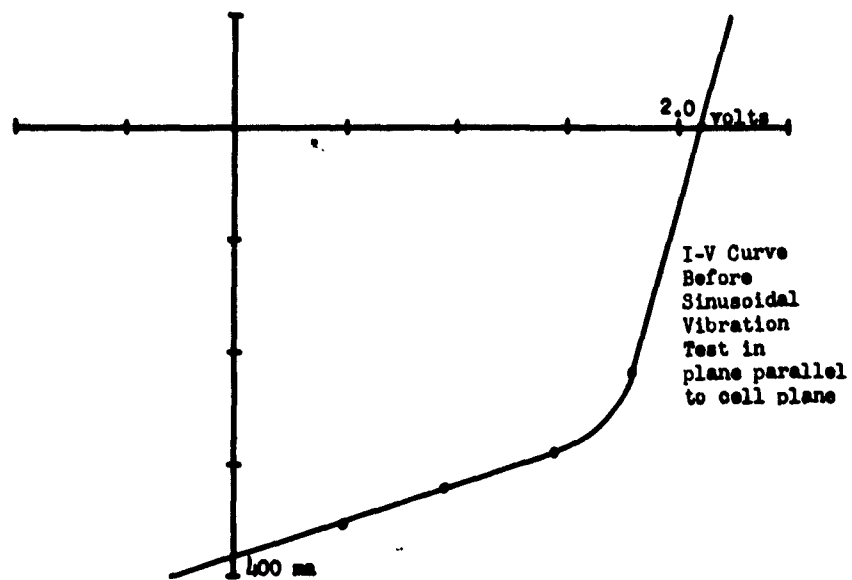


Figure 12c

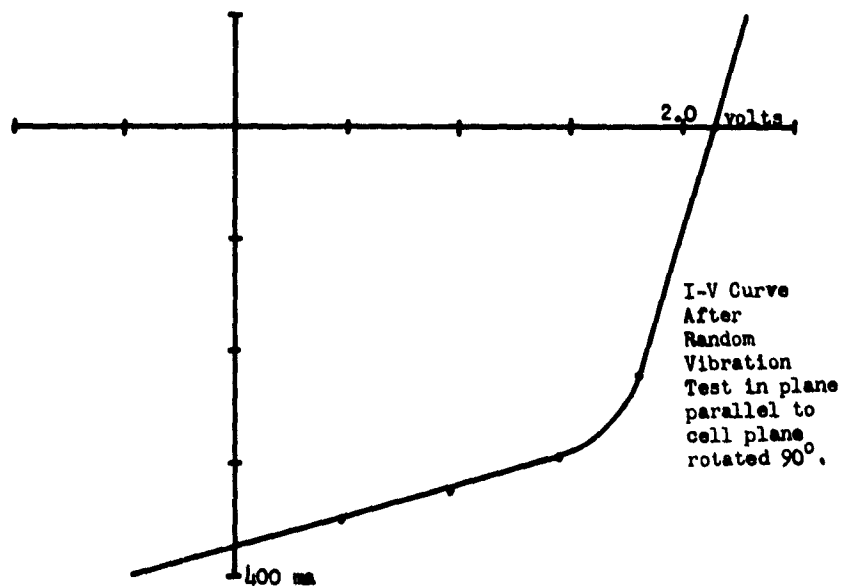
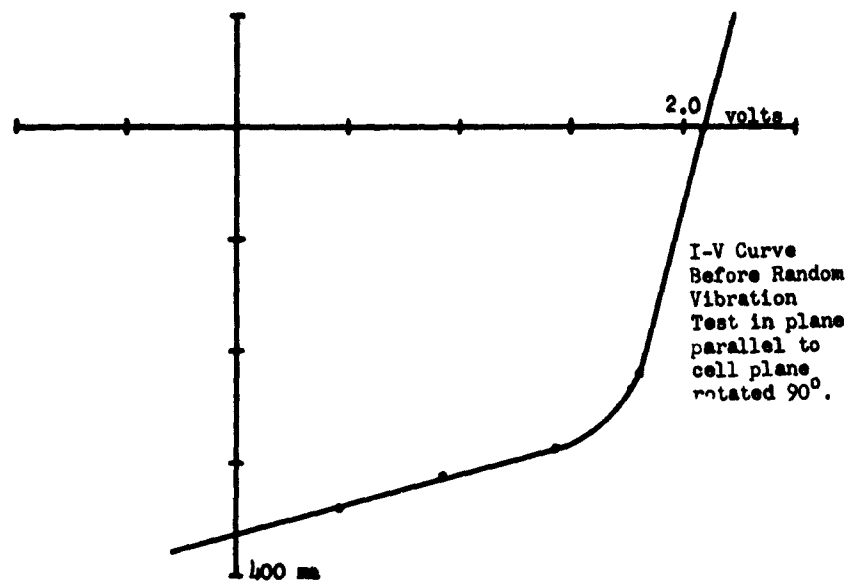


Figure 13

TABLE IV
RANDOM VIBRATION TEST DATA

	<u>Time of Test</u>	<u>Load Resistance in Ohms</u>	<u>Voltage</u>	<u>Current in ma</u>
Array No. 289MN	Before Random Noise Test	-	2.15	0
		8.2	1.81	221
		5.0	1.46	292
		3.0	.97	323
		1.4	.49	350
	After Random Noise Test	-	2.1	0
		8.2	1.75	214
		5.0	1.45	290
		3.0	.97	324
		1.4	.49	350

On the basis of these data reported here and in the first quarterly report⁽¹⁾ the panels are expected to perform satisfactorily during the orbital experiment.

Cell and Array Construction

Encapsulating Materials

The selection of the best materials for the encapsulation of the CdS solar cells was somewhat difficult due to the great lack of agreement concerning the performance of the plastic film materials in space.

Originally, Mylar was chosen because of its strength, clarity, and radiation resistance, but later information indicated a darkening by ultraviolet radiation in space after a short period of exposure. It was learned that Mylar could be obtained with a coating on one side that was capable of absorbing ultraviolet. This material was obtained and attempts were made to laminate it to the cells but with no success. It was necessary to develop process modifications to enable its use. This was accomplished in sufficient time to permit its use for all but two of the twelve arrays needed for the four orbital panels.

As mentioned in the last quarterly report⁽¹⁾, polypropylene bi-axially oriented film has been reported to remain essentially clear under space conditions, but all attempts to laminate the thin film CdS solar cells with this material have been negative.

Other materials are also being investigated in an attempt to circumvent this difficulty. One such material is called Phenoxy-8, which reportedly can

~~be used alone or as an adhesive~~ in conjunction with other plastics. It was felt that this material could serve as the encapsulating or outer plastic and as the adhesive needed to hold the collector grid in place. Unfortunately, satisfactory plastic bonding is accomplished at 180°F which is 20° less than that required for orbital use. Higher laminating temperatures cause the film to become cloudy as in the case of polypropylene. Some success was achieved, however, when the Phenoxy-8 was used with Mylar as a substitute for the Capran layer. The bond and clarity appeared to be equivalent in all respects to that obtained with Capran. Attempts to laminate Phenoxy-8 with polypropylene in a similar manner resulted in poor bonding and cloudy films.

Samples of Mylar with an adhesive (GT 300) layer have been obtained from the G. T. Schjeldahl Company and are being tested. Successful laminations of Mylar to Mylar using this material were made at 65°F less than that required for Mylar-Capran-Mylar laminations. This adhesive and others shall be used in experiments with polypropylene. The GT 300 adhesive is claimed to be unaffected by UV or other radiations. Success in this area will probably result in somewhat lighter package, in addition to an increased space life.

At the request of the contract monitor, a special cell capable of withstanding any type of weather condition was to be made in which weight and flexibility were not of major consideration. The cell shall be used in an experiment comparing the cell output on the surface of the earth with the output at a high altitude. The cell designed for this purpose, 1 inch x 1 inch, was encapsulated in the regular Mylar-Capran envelope, which in turn was cemented between two $\frac{1}{4}$ inch thick sheets of Lucite. Two terminals were also sandwiched in between the Lucite layers such that they partially protruded at the side. The data obtained on this unit taken in collimated sunlight and under equivalent terrestrial tungsten light and is given in Table V.

TABLE V

DATA ON LUCITE ENCAPSULATED CELL

<u>Cell No.</u>	<u>% Efficiency-Tungsten-</u>	<u>% Efficiency-Sunlight*</u>
387 MNL	3.5	3.6

* Sunlight at time of measurement was 74.5 mw/cm². Value reported was adjusted to 100 mw/cm².

Pilot Line

Continued operation of the pilot line produced 412 various sized cells. Of this amount many were subsequently laminated for life tests, orbital evaluation tests, radiation samples and various mechanical tests. A table of values is included, listing both cells and laminated arrays. The table shows that the

average cell efficiency has dropped and that the scrap rate increased considerably. During this period considerable difficulty has occurred in evaporation due to poor thermocouple readings, in barrier plating due to a faulty plating supply, and insufficient rinsing because of contaminated rinse water. A closer control of variables will be maintained in an effort to raise the efficiency level of the cells to where they were previously.

TABLE VI
CELL AND ARRAY DATA

CELLS

<u>No. of Cells</u>	<u>Size</u>	<u>OCV</u>	<u>Efficiency</u>			<u>Scrap</u>
			<u>Min</u>	<u>Max</u>	<u>Avg</u>	
295	1" x 3"	.495	1.0	3.3	2.00	87
117	3" x 3"	.497	1.0	2.8	1.97	37

ARRAYS

<u>No. of Arrays</u>	<u>Size</u>	<u>Description</u>	<u>Efficiency</u>		
			<u>Min</u>	<u>Max</u>	<u>Avg.</u>
7	1" x 3"	Life tests	2.6	3.4	3.1
15	6" x 6"	Orbital evaluation	1.5	3.1	2.4
3	1" x 1"	Lucite	2.8	3.7	3.2
3	1" x 1"	Lucite	Mechanical samples		
24	1cm x 1cm	Radiation samples	.4	3.3	2.1
19	Misc. sizes	Mechanical samples			

Cell Contacting

Although the present technique for the lamination of CdS film cells enjoys a fair degree of standardization and reproducibility efforts are continuing to find an improved and a more economical collector grid. The grids presently used are directly responsible for increased collector efficiency and an increase in energy conversion efficiency. However, other materials may possibly operate as well and may be more economical.

We are presently engaged in evaluation experiments for the materials that are available. Using the pressure test unit reported earlier, gold and silver grids appear to be essentially equivalent and superior to nickel and copper collector grids.

In another test, four 3" x 3" cells were contacted, one half at a time, first with gold and then with silver in the pressure test unit. Again very

little difference was noted. However, on lamination of these cells the gold has shown about a 20% improvement over the silver. The number of samples was too small to permit a definite conclusion to be reached.

Another test was made using a 3" x 3" cell that had a uniform efficiency over its entire surface. This cell was laminated with silver, gold, nickel, and copper with each grid covering approximately one-fourth of the barrier area. The results of this test has shown that nickel is superior to copper and silver and is nearly as effective as gold. The data are given in Table VII.

TABLE VII

EFFECTIVENESS OF GRID MATERIALS

<u>Grid Type</u>	<u>V_{oc}</u>	<u>I_{sc}</u>	<u>Power</u>	<u>Area</u>	<u>Eff.</u>
Copper	0.44V	85ma	19.10mw	10.85cm ²	1.76%
Silver	0.45V	80ma	20.96mw	11.12cm ²	1.89%
Nickel	0.47V	83ma	21.80mw	10.85cm ²	2.01%
Gold	0.44V	90ma	23.76mw	11.12cm ²	2.12%

This indicates that it may be possible to collect the current effectively with a more economical material than the silver or gold. Many possibilities exist in this area.

Cell Stability

The stability of the CdS thin film cell and its package in both terrestrial and extraterrestrial environments are of great importance. As mentioned in the orbital evaluation section of this report, attention was focused on the encapsulating plastics used for the panels, since any damage suffered by the plastic could result in a loss of power or complete failure. This was discussed in that section and no further mention will be made here.

Several small samples were sent to the Naval Research Center for electron and proton damage, but official results have not been received as of the writing of this report. A verbal report indicated that the CdS cells suffered very little damage and that this damage may have been the plastic rather than the CdS itself. A report on radiation damage, no doubt, will be available for the next quarterly report.

Other Methods of Film Formation

The investigation of methods other than evaporation for the formation of

thin films of CdS has been directed toward electrophoretic deposition and the subsequent need for the sintering or recrystallization of the deposits. The deposition takes place in an electrolytic cell filled with an organic liquid that will maintain a suspension of colloidal CdS powder. Molybdenum electrodes are used since it is desired to use this metal as a substrate.

Attempts to form a CdS film suitable for photovoltaic use has followed a three step pattern. First is the preparation of the suspensions, second, the deposition of the CdS, and third, the subsequent treatment of the deposit.

In order to obtain a satisfactory colloidal suspension it has been found necessary to pulverize the CdS powder. This has been accomplished by ball milling and by ultrasonic vibration. The latter method appears to be the better because of ease of use and convenience, and it apparently produces a finer particle size in far less time. The procedure followed throughout the experiments listed in Table VIII was as follows: One gram of CdS powder per 100 ml of Isopropyl Alcohol was mixed together and subjected to ultrasonic vibrations for about 15 minutes. During the pulverization, an additive, usually a wetting agent, was placed in the solution to insure thorough mixing in the suspension. The particle size of the suspensoid was not measured.

The equipment used for deposition includes a variable d-c power supply with a capacity of 460 volts and .5 ampere, and a beaker fitted with a cover with attached molybdenum electrodes spaced about 1 1/8" apart. Operation consisted merely of transferring the suspension media to the beaker, inserting the electrodes and then applying the required voltage. Only four substances were tried as the suspension media. Undoubtedly, more could have been tried, but the good results of the Isopropyl Alcohol did not seem to justify further investigation at this time. Preliminary tests also showed that satisfactory deposits were unobtainable at the voltage level available unless an additive was used. The experiments listed in Table VIII show the effect of additives, voltage, and time upon the film formation. Not all of the experiments are listed.

The deposits as formed, varied in thickness, density, texture, and evenness, but one thing in common with all of the deposits was their adherence to the substrates. Flexing of the substrates does not loosen the film layers, but in all cases they could very easily be wiped off. Heat treatment of the films in attempts to increase adhesion to the substrates, cause recrystallization and conversion to suitable photovoltaic films was unsuccessful. Table IX lists the experiments performed for that purpose.

The adhesion to the substrate did improve considerably, but no evidence of film crystallization was evident. The only crystallization that did occur was on a control sample of a previously evaporated film deposit on which single crystals were observed to form. It is possible that these particles are not properly oriented or that the necessary temperature and atmosphere have not been found for recrystallization.

TABLE VIIIELECTROPHORETIC DEPOSITION DATA

<u>Additive</u>	<u>Voltage</u>	<u>Time</u>	<u>Remarks</u>
1. Dural	460 V.	5 min.	Thin uneven deposit-considerable bubbling
2. Dural	460 V.	5 min.	Heavy-fairly even deposit
3. Dural	460 V.	5 min.	Thin uneven-heavy at edges
4. Cornstarch	450 V.	5 min.	Traces of deposit
5. Ultrawet "E"	450 V.	25 min.	Thin-uneven deposits
6. Dural	450 V.	1 min.	Smooth-fairly even
	100 V.	9 min.	
7. Dural	450 V.	2 min.	Smooth-even deposit
	150 V.	3 min.	
*8. Cornstarch	450 V.	10 min.	Unsatisfactory deposit
*9. Dural	450 V.	10 min.	Unsatisfactory deposit
**10. Cornstarch	450 V.	10 min.	No deposit
**11. Dural	450 V.	10 min.	No deposit
12. Ammonium Hydroxide	450 V.	10 min.	No deposit
13. Sodium Hydroxide	450 V.	10 min.	No deposit
14. Sodium Hydroxide + Dural	450 V.	10 min.	No deposit
15. "Wisk"	450 V.	2 min.	Even-coarse deposit
	150 V.	2 min.	
16. "Wisk"	300 V.	1 min.	Even-less coarse
	100 V.	3 min.	
17. "Wisk"	250 V.	30 sec.	Thin porous
	75 V.	4 min.	
18. "Wisk"	300 V.	2 min.	Smooth-even deposit
19. "Wisk" concent.	300 V.	2 min.	Smooth-even deposit
20. "Wisk" concent.	200 V.	2 min.	Smooth-even deposit

- Note:
1. The suspension media in all cases except where noted was Isopropyl Alcohol.
 2. The substrate or electrode was molybdenum.
 3. The distance between electrodes remained at about 1 1/8" for all tests.
- * Acetone as suspension medium.
 ** Methanol as suspension medium.

TABLE IX

HEAT TREATMENT OF ELECTROPHORETIC DEPOSITS

<u>HEATING CONDITIONS</u>			<u>REMARKS</u>
<u>Temp.</u>	<u>Time</u>	<u>Atmosphere</u>	
1. Deposited film heated under bunsen burner			Formed CdO and Molybdenum Oxide.
2. 550°C.	1 hr.	Argon	3-Deposited substrates 1-Evaporated substrate No evidence of the formation of crystallites on either type.
3. 900°C.	16 hr.	Argon	Same as #2 except practically everything evaporated leaving moly oxide substrates.
4. 750°C.	16 hr.	Argon	Same result as #3.
5. 550°C.	4 hr.	Argon	2-Evaporated substrates-one coated with silver as activator. 2-Deposited substrates-single crystals formed on evaporated substrate coated with silver.
6. 550°C.	18 hr.	Argon	-Deposited substrates only No evidence of crystallization.

PART II - MATERIALS RESEARCH

Purification of Cadmium Sulfide

Since purification of CdS itself is difficult, it was decided to form the sulfide from very high purity cadmium and sulfur. Cadmium, although available in a state of fairly high purity, (99.9999%) may well be further purified by vacuum distillation and zone refining. Any H_2S needed for this effort could be purified by passing through a purification train. Distillation of the cadmium under vacuum should remove traces of impurities, mostly copper and magnesium that are not easily removed by zone refining.

A quartz still has been constructed for this purpose, and is in the form of an inverted U with a flask on one end that serves as a melting chamber for the cadmium rods. During operation it is intended that the liquid Cd be forced up by atmospheric pressure into another flask which has been heated by a mantle to about $390^{\circ}C$. The vapor pressure above the cadmium at this point should be about 1 mm Hg, the cadmium vapor should distill over to the other side of the U where it will condense and slowly run down to a receiving flask on the bottom. From this it will drain out to a tube or boat. An oven to accommodate this still is now under construction. The oven is designed to hold at $340^{\circ}C$ (m.p. of cadmium is $320^{\circ}C$) and will be flushed by nitrogen to exclude oxygen.

The techniques of further zone refining cadmium are being developed. For this purpose cadmium is held in a quartz boat which is in turn placed in a vycor tube. The molten zone is produced by 3 turns of Tophet C metal alloy wrapped around the vycor tube. This in turn, has an aluminum radiation shield around it to reflect the heat. The power is provided by a transformer.

Initially the zone refining was done under argon which, however, was found to contain a small amount of O_2 or H_2O , thus causing the cadmium to be oxidized. Hydrogen was tried, but unfortunately, it also contained O_2 or H_2O which caused a film of oxide to form on top of the bar. This film was removed during the passage of the molten zone, but formed again on the cool portion of the cadmium. A dry ice trap was ineffective in removing the water from the H_2 . Drying with P_2O_5 or Decoxo units will be tried next.

A bar of reagent grade cadmium that was zone refined with 4 passes showed the analysis given in Table X. Thus zone refining appeared effective in removing most of the impurities from the Cadmium. Some aluminum and calcium contamination was introduced apparently from the quartz boat.

A train for the purification of H_2S which was used previously in the preparation of CdS will be used again in subsequent experiments.

When the purified cadmium and H_2S are prepared, they will be reacted in a quartz tube at about $1250^{\circ}C$ in an attempt to form CdS crystals. Since CdS crystals are grown at this temperature from sintered stock, it was deemed advisable to analyze, by mass spectrographic procedures, the seed pile and crystal product in an attempt to determine the impurities that pass over with the CdS. Four samples were selected as representing typical production.

TABLE X
ZONE REFINED CD ANALYSIS

<u>Element</u>	<u>Original</u>	<u>Front</u>	<u>Middle</u>	<u>Last</u>
Al	Ft+	T-	T+	W-
Sb				Ft+
Bi		VFT	VFT-	VFT+
Ca	FT	FT+	T	T+
Cu	T-	FT	FT+	T
Ga	VFT+	VFT-	VFT+	VFT
Fe	FT	FT	FT+	FT+
Pb	FT+	FT-	FT	W+
Mg	FT	FT+	T+	T
Mn	VFT-	VFT-	VFT	VFT+
Ni	VFT	VFT-	VFT	FT-
Si	T-	T	W-	W
Ag	FT-	FT	FT	FT-
Na			T	T
Su				Vft
Ti	VFT+	FT-	FT	FT+

The procedure in making the samples was to heat sintered CdS placed in the middle of the mullite tube. The CdS sublimed and condensed at the ends of the tube. Sample O-114 P was made from G. E. Luminescent Grade CdS, Lot No. 54. It was heated 100 hours at 1270°C. The primary crystal was light amber, clean, excellent clarity, with a few fractures in the bottom. Its rating was L-O-O. No dopant was used. Sample 1-116 P was made from sintered G. E. luminescent grade CdS, Lot No. 126. 0.03% Indium as InCl_3 was added as a dopant. It was heated at 1280°C. The primary crystal was dark amber and had 7 fractures. Sample OS-99 P was made from sintered CdS, G. E. luminescent grade, Lot No. 54. It was heated 96 hours at 1250°C. There was no dopant but the crystals grew under a stream of H_2S . The primary crystal was light amber and clear. Sample OS-111 RF is a sample of the residual feed-pile. G. E. luminescent grade CdS, Lot No. 126 was used in this run. It was heated 150 hours at 1250°C. under H_2S . No dopant was used.

The first 2 samples were made under argon, the last 2 under H_2S . It may be that the H_2S helps impurities pass over from the feed pile to the growing crystals. However, the amounts of impurities are too high in any case. Sodium, potassium, and lithium will be three impurities that will have to be removed in the zone refining and distillation. Copper, calcium, magnesium, and carbon will also have to be watched closely. Further samples will be submitted of cadmium before and after purification, and of CdS before sintering in order to determine what impurities are present in the starting material. These four samples of CdS were sent to the Bell and Howell Research Center, Pasadena, California, for mass spectrographic analysis. The results are given in Table XI.

TABLE XI
MASS SPECTROGRAPHIC ANALYSIS OF CDS

<u>Element</u>	<u>Detection Limit</u>	<u>0-114 P</u> (Argon grown)	<u>1-116 P</u> (Argon grown Indian doped)	<u>OS-99 P</u> (H ₂ S grown)	<u>CS-111 RF</u> (H ₂ S grown)
In	0.06	N.D.	35	N.D.	N.D.
Ga	0.08	N.D.	N.D.	0.5	8
Cu	0.06	1.3	2	15	35
Cd	0.05	N.D.	0.9	6	N.D.
V	0.04	0.5*	N.D.	1	N.D.
Ca	0.03	6	0.7	90	62
K	0.04	40	4	300	600
Cl	0.04	0.2	N.D.	N.D.	3
P	0.03	N.D.	N.D.	0.05	N.D.
Al	0.06	0.1	N.D.	6	10
Mg	0.03	1.1	1.3	5	10
Na	0.03	34	90	1000	650
N	0.02	0.03	1.1	N.D.	0.5
C	0.02	4	87	7*	550*
Li	0.02	18	6	170	1500
H	0.010	0.9	12	0.05	0.05
Total		106.13	205.0	1600.6	3428.55

Impurities are given in ppm atomic. ND means not detected. *Not consistent on all exposures. Either it is a surface contaminant or lies in isolated pockets. Impurities not listed are less than 1 ppm except for O, Fe and Zn, which are not given because of Cd and S interference. Concentrations are corrected for the mass dependency of the photographic plate.

Film Structure Studies

Earlier work on the formations of barriers on CdS grains growth films has indicated a difference in the darkening of different grains. This, combined with the observed correlation of darkening vs. photovoltaic efficiency vs crystal orientation on single crystal cells, has led to a program of grain growth improvement, grain orientation studies, and crystal surface studies. The grain growth improvement work has been involved with (a) developing techniques for the growth of grains, and (b) uncovering those parameters that affect the growth of grains. The grain orientation studies have involved the development and/or employment of tools and techniques by which grain

orientation can be determined. The crystal surface studies have dealt with the problem of determining the condition of CdS surfaces in various environments.

The techniques by which grain growth have been attempted up until this report period include (a) a fast heat treatment in an open atmosphere using a bunsen burner flame as the heat source, (b) the heating of films in atmospheres and under vacuum by the passing of current through the molybdenum substrates, and (c) the annealing of films in a high vacuum using a heating tape or wire ribbon as the heat source. The best grain growth, i. e. the films on which the largest grains have been observed, has occurred on films annealed by the method mentioned under (c) above. The growth of grains by this method has, however, varied considerably in quality and reproducibility has not as yet been obtained. Method (a) provides the most reproducible results. Attempts to grow grains during this report period by the heating of films sealed in quartz tubes under high vacuum ($\approx 10^{-6}$ mm Hg) has not resulted in any improvement. Control of the temperature of the heating source has been difficult and the procedure of sealing up quartz tubes has been both expensive and time consuming. Six growth experiments were performed in this manner with no notice of improvement of grain growth. Further growth experiments have been made using a chromel heating strip wrapped around an open ended quartz tube. The heating strip, in this case, was placed inside an evaporator so that the experiments could be performed under vacuum conditions. Twelve runs have been made. Short runs at high temperatures have resulted in the evaporation of excessive amounts of CdS. Longer runs at low temperatures revealed no observable grain growth even under high microscopic examination. Intermediate temperature runs for short time periods have revealed some growth but the quality of the growth is rather poor. Longer runs have not been undertaken due to excessive heating of the bell jar of the evaporator. Heat shields have been made and are presently being assembled in the evaporator. Long runs at intermediate temperatures are planned.

From a more basic point of view an understanding of the influence of deliberately applied stresses to the films before annealing, of impurity additions on the interfacial surface energies, and of dislocation content on the mobility of interfaces is deemed necessary if grains of larger size are to be grown. Attempts will be made to initiate such a program when experimental techniques are refined enough to guarantee some sort of a reproducible starting point for such a study.

Crystal orientation studies are being employed using x-ray pole figure analysis, electron microscope studies, and light-figure studies. The pole figure analysis was carried out by the Analytical Section of the Harshaw Chemical Company while certain light-figure studies of single crystals have been made in this laboratory. A microscope light figure is also being constructed to determine grain orientation on grain growth films. The results are discussed in the following section. The electron microscope studies are also being performed by the Analytical Section.

An attempt was made to obtain a transmission electromicrograph of a grain growth sample but the sample evaporated. Leaks in the equipment have postponed further work. Graphite replicas have been prepared and electromicrographs will be made of grain growth samples when the equipment is reassembled.

The light figure studies have been aimed at the development of a technique by which grain orientation can be uniquely determined. In order to develop etch pit shapes that are unique to specific planes many different etchants have been used. A few of these have been reported in previous reports. Table XII gives a list of other etchants that have been tried and conclusions regarding the results. The vacuum etchant gives an indication of being the most useful etchants for determining grain orientation. Orientation studies of grains on films annealed in a vacuum will be made using the microscope light-figure apparatus when it becomes available.

Many of the principles upon which the orientation studies of CdS crystals is based can be found in the published version of the presentation "Crystal Morphology in Evaporation, Equilibrium and Growth in the Vapor Phase." This presentation was given at "The International Symposium on Condensation and Evaporation of Solids.", which was held in Dayton on September 12-14, 1962. A copy has been included as an appendix. The kinetic evaporation and condensation equations are based on a study of CdS. The polytype studies, referred to S₁C in the paper, are based on the known existence of polytypism in many of the II-VI compounds. A more detailed account of polytypism as applied to II-VI compounds is given in the third quarterly report on Contract AF 33(657)-7916.

The importance of polytypism in the study of II-VI compounds lies in the association of photovoltage and electroluminescence with stacking faults in crystals. Polytypism, in turn, results, from the systematic introduction of stacking faults in a basic sphalerite type lattice, by twinning parallel to a single [111] direction. This association deserves special attention from a device design stand point since it is conceivable that through a deliberate introduction of stacking faults into a crystal lattice the photovoltage of that device can be controlled. In a CdS solar cell, for example, it is anticipated that stacking faults can be introduced into the lattice by the addition of zinc or tellurium.

The crystal surface studies are also based on the principles given in the attached paper. The results of CdS vapor etching is included along with that of other II-VI compounds. Results are given in previous reports under this contract for crystals etched in various solution etchants. A comparison of the results shows a definite difference between vapor etched patterns and solution etched patterns and as a result, tentative conclusions concerning the nature of the surfaces can be made. There is still not a sufficient amount of data to draw a final conclusion. Further etching at high temperatures in various vapors and in vacuum are contemplated.

TABLE XII
ETCHANTS FOR CDS

<u>Etchant</u>	<u>Time</u>	<u>Temperature</u>	<u>Results</u>
1-pyridine, 2-HCl	5 secs.	R.T.	(0001), (10 $\bar{1}\bar{1}$) and zones between them. Signs of (0 $\bar{1}$ 01) and (11 $\bar{2}$ 1). Also, zone between (1010) - (0110) and (10 $\bar{1}\bar{1}$)-(01 $\bar{1}\bar{1}$).
1-butylamine, 2-HCl	45 min.	R.T.	Faint pattern. (10 $\bar{1}\bar{1}$). Zone between (1010)-(0110) and (10 $\bar{1}\bar{1}$)-(01 $\bar{1}\bar{1}$). Incomplete zone from (10 $\bar{1}\bar{1}$) to (0001).
1-triethylamine	30 min.	R.T.	Clear pattern. (0001) and (10 $\bar{1}\bar{1}$). Very complex pyramidal and prismatic area pattern.
1-tetradimethylaminodiborate 2-HCl	3 min.	R.T.	Clear pattern. (0001) and (10 $\bar{1}\bar{1}$). Very complex pyramidal and prismatic area pattern.
1-amino acid 3-dilute HCl	4 min.	HOT	Clear pattern. (0001) and (10 $\bar{1}\bar{1}$). Very complex pyramidal and prismatic area pattern.
1-amino acid 2-HCl	4 min.	R.T.	Faint pattern. (0001) and (10 $\bar{1}\bar{1}$). Very complex pyramidal and prismatic area pattern.
H ₃ PO ₄	40 hrs.	R.T.	No Results
H ₃ PO ₄	5 hrs.	80°C.	Standard HCl pattern plus prismatic zone.
H ₂ SO ₄	8 hrs.	HOT	Double star pattern plus prismatic zone.
1-H ₂ SO ₄ 1-H ₂ CrO ₄	8 hrs.	R.T.	Faint pattern. Standard HCl pattern plus prismatic zone.
NH ₄ OH	2 weeks	R.T.	No results
NH ₄ Cl	2 weeks	R.T.	No results
1-KCN, 1-H ₂ O ₂	2 weeks	R.T.	No results
1-KCN, 1-KOH	2 weeks	R.T.	No results
Vacuum ($\approx 10^{-3}$ mm Hg)	2 hrs.	900°C	Clear double star etch with an added number of pyramidal planes.

Some mention should be made of the possible correlation between equilibrium forms and Brillouin zones. A great deal of similarity exists between the methods of calculating and constructing first nearest neighbor equilibrium forms and the first Brillouin zone. The calculations for equilibrium forms is based on the detachment energy of atoms, ions, molecules, etc. in the equilibrium position of crystals. In Brillouin zone calculations this corresponds to the removal (i.e. evaporation) of the last electron needed to fill the Brillouin zone (for a semiconductor i.e. one may say from the Fermi level to the bottom of the conduction band.) Thus, in a manner analogous to equilibrium form calculations, Brillouin zone calculations might be possible by utilizing various ratios of ionization energy of electrons associated with cations and anions. This raises the possibility of the existence of Brillouin zones which exhibit polarity. A simple one dimensional picture of this is given in Figure 14. It is realized that in this one-dimensional model, a symmetry center is required. It may not be true for the two-or three-dimensional cases. In a similar manner, Brillouin zones showing anisotropy can be developed by the consideration of varying ratios of c-directional ionization energies. This is shown in Figure 15. In this case, however, if both atoms are identical, no center of symmetry is removed.

These considerations may prove to be of importance in matters concerning the existence of polytypism in CdS or even of the existence of stacking faults in this material. The explanation of photovoltages associated with stacking faults may be in the considerations presented here. A detailed look at the quantum mechanics involved appears to be in order to prove or disprove such concepts.

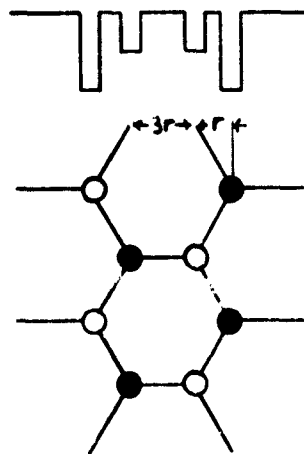


FIGURE 14

The Kuper-Pennay Model No. 1 (one-dimensional) of an electron moving in a periodic structure in which the electron associated with one atom of a compound semiconductor is bonded more strongly than the electron associated with the other atom. The model contains an easy direction of motion and a difficult direction of motion. In two dimensions, three easy and three difficult directions are possible. The resultant Brillouin zone should show a polarity.



FIGURE 15

The Kronig-Penney Model No. 2 (one-dimensional) of a compound structure in which c-directional electrons are bonded more strongly to the lattice than a-directional electrons.

Pole Figures of CdS Films on Glass and Molybdenum

In connection with the preparation of CdS thin film photovoltaic cells, efforts have been directed towards film growth, perfection, and their relation to efficiency. A preliminary study of several features of thin film deposition was considered necessary.

The deposition of CdS from the vapor state onto a substrate leads to a preferred orientation of the crystalline grains. Generally it has been found that (00 \cdot 2) planes deposit nearly parallel to the plane of the substrate. However, the orientation of (00 \cdot 2) planes is not perfect but assumes a range of angles with respect to the substrate plane. The present work relates to actual production cells formed on glass and molybdenum substrates.

Figure 16 is a pole figure of (00 \cdot 2) planes from a CdS film deposited on a glass substrate. The film was peeled from the glass and examined on the substrate side by reflection. The pole figure shows the most frequent tilt of the (00 \cdot 2) planes to be at an angle of several degrees from the substrate plane. A substantial amount of tilt appears at angles as large as 20°. This manner of growth may be similar to that reported by Reynolds and Greene⁽²⁾, for type II crystals of CdS grown from the vapor on a quartz substrate. It may indicate that the nucleation mode is the same in the growth of a single crystal or a polycrystalline film. Subsequent growth would depend on the grain interfacial energies and could be very different in a single crystal grain or an oriented polycrystalline film. The nearly symmetrical arrangement of the pole figure indicates that similar fractions of (00 \cdot 2) planes are located in each azimuthal direction in the plane of the film. Figure 17 is a pole figure from the opposite side of the CdS film. Since the two inner regions are reversed in intensity and the figure is no longer symmetrical about the substrate normal, the fraction of (00 \cdot 2) planes oriented at a fixed angle to the substrate plane has now changed. The fraction at a certain azimuth has apparently changed but this may be an artifact. While these effects are difficult to assess quantitatively and represent only one sample, they reflect real differences between the two sides of the film.

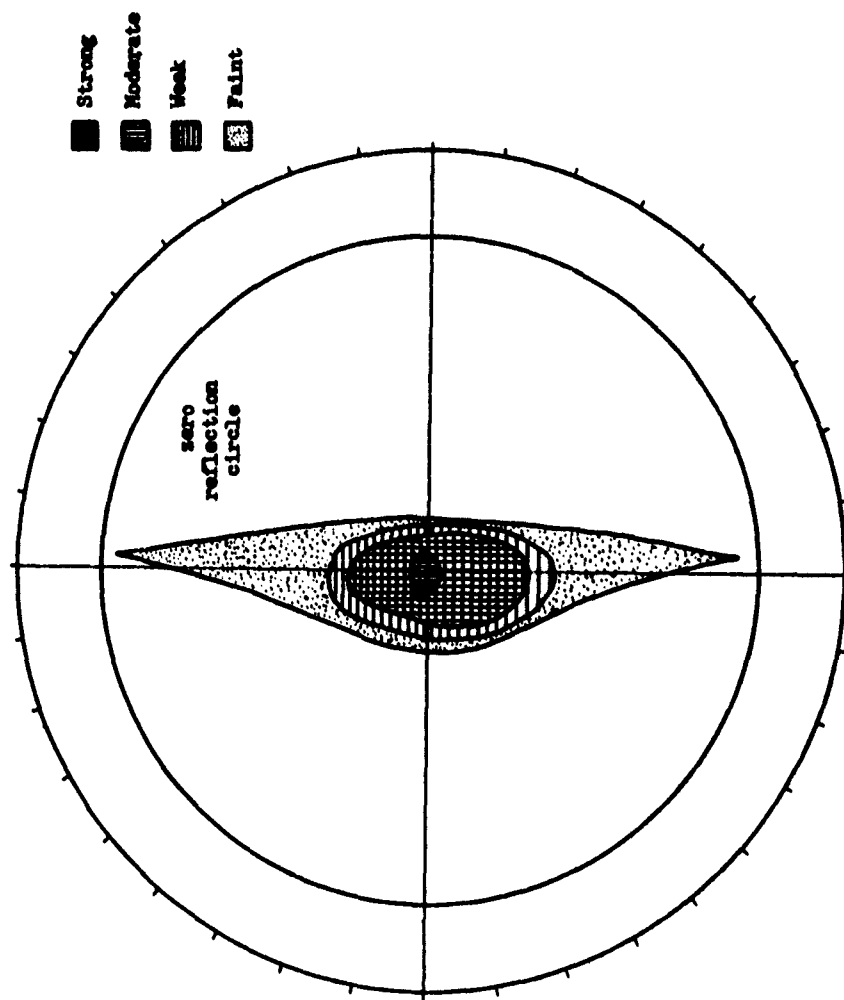


Figure 16: Pole Figure of (00.2) Planes of CdS, Glass Substrate Side, Normal to Substrate at Center of Figure.

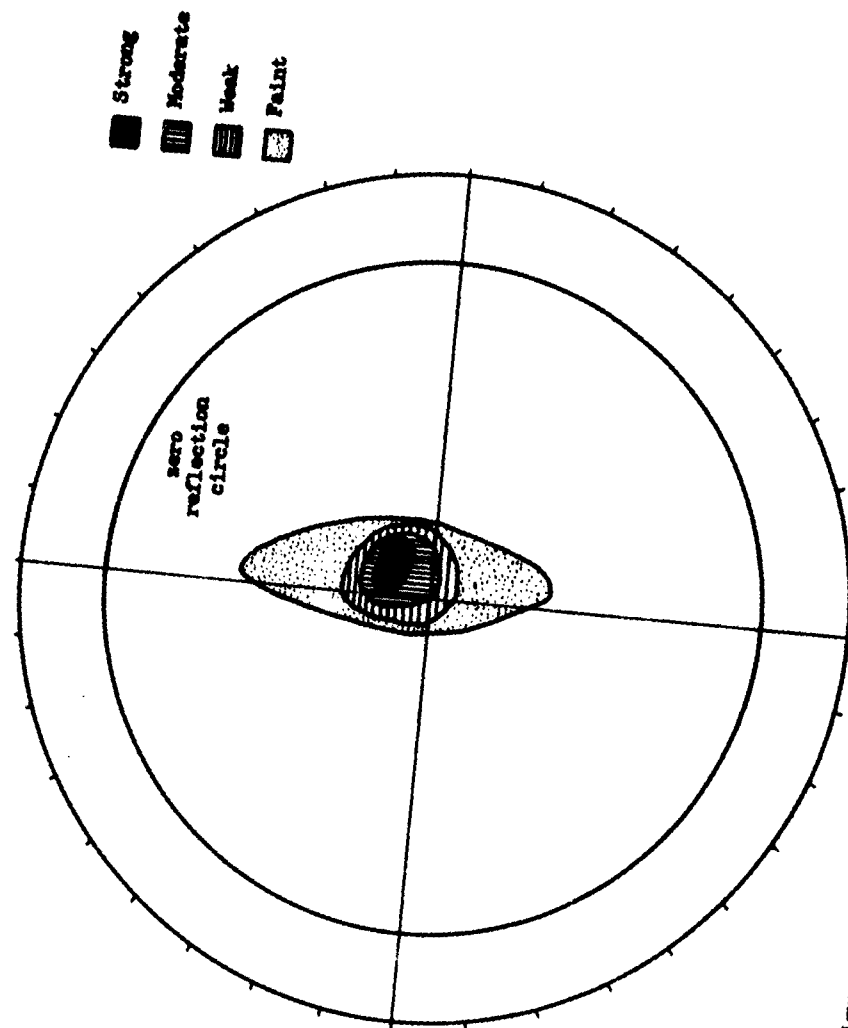


Figure 17: Pole Figure of (00.2) Planes of CdS, Surface Side, Normal to Glass Substrate at Center of Figure.

Figures 18 and 19 are pole figures for (00·2) planes of CdS. The CdS film was peeled from the molybdenum substrate and examined on both sides by a reflection technique using filtered radiation. The side of the CdS close to the substrate, Figure 18, showed almost symmetrical arrangement of (00·2) poles about the normal to the substrate. The intensity data shows that the majority of planes of type (00·1) are parallel to the substrate although some are again tilted up to angles of 15°. The side of the CdS away from the substrate, Figure 19, showed a noticeable different pole figure. In this case the majority of the (00·1) planes are tilted a few degrees from the normal to the substrate. This probably reflects the changing orientation of the CdS growth layers or the fact that a perfect epitaxial growth does not persist over the CdS film thickness. The relation between the substrate and the CdS deposit is not clear at this time because definite studies have not been performed. For a body centered cubic metal such as molybdenum, the rolling texture of thin sheets of the type being used is (001) [011]. This is not perfect but many reasons could be formulated for the fact that CdS still deposits in an oriented fashion. Our limited work has shown that the influence of the substrate is probably not too significant in present epitaxial growth since the results on glass and molybdenum are comparable. However this may only be true because the other growth conditions are nearly equal. Thus substrate temperature, vacuum, rate of evaporation, and geometry have to be judged as well as the substrate condition. If the proper combination of growth variables can be found, a more perfect orientation may result and the efficiency of thin film cells may be substantially increased. This emphasizes the importance of these studies and the genuine possibilities of achieving essentially the same efficiency as the single crystal cells.

PART III BASIC BARRIER STUDIES

The spectral response of the CdS solar cell can be used to provide information concerning the nature of the photovoltaic mechanism and can also predict the performance of the cell under illumination of known spectral distribution. Work in this quarter has been mainly directed toward the latter aspect.

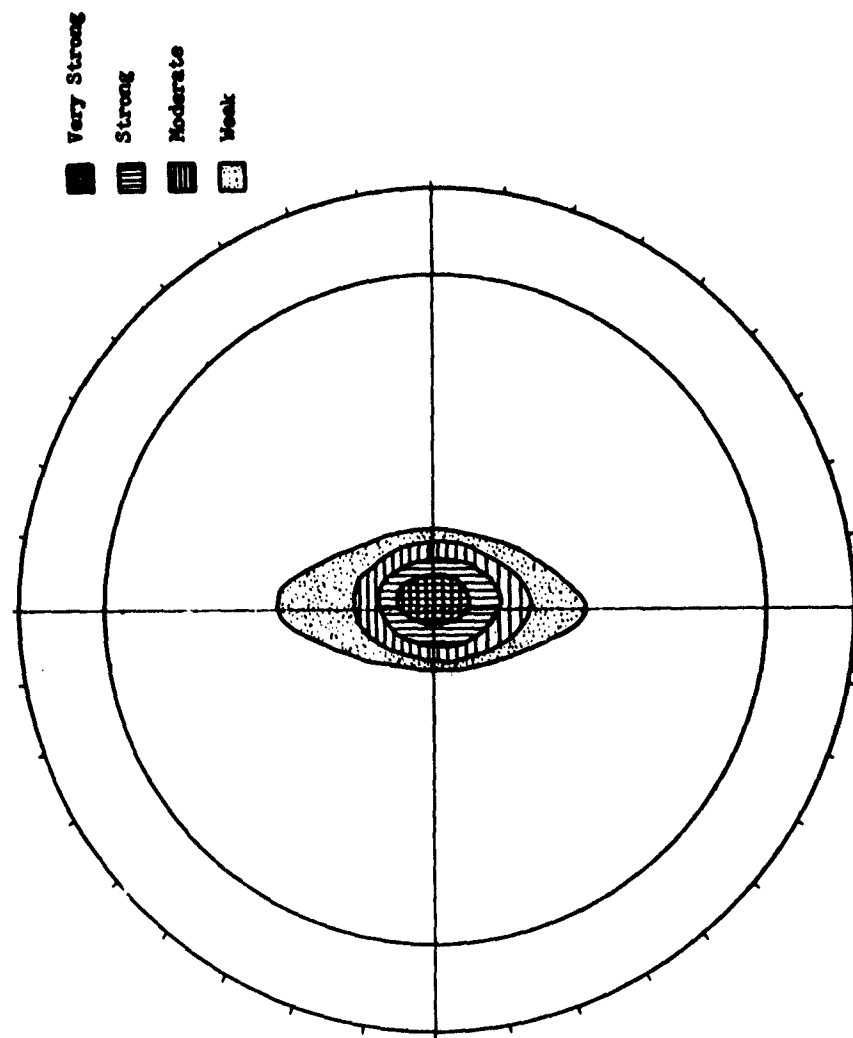
Analysis and synthesis of an expected short circuit current has been performed on two front wall cells. The analysis consists of determining the quantum yield Q in electrons per photon as a function of wavelength, whereas the expected current can be calculated as follows. The quantum yield at a given wavelength is multiplied by the illumination photon flux per unit wavelength interval at the wavelength. This operation is performed over the wavelength interval from zero to infinity, forming a function which is the generated short circuit current per unit wavelength interval. The integral of this function from zero to infinity is then the calculated short circuit current, as expressed in the following equation:

$$J = \int_0^{\infty} Q(\lambda) F(\lambda) d(\lambda)$$

J = Short circuit current in electrons/cm² sec.

Q = Quantum yield in electrons/photon

F = Illumination photon flux in photons/cm² sec. x unit wavelength



41

Figure 18: Pole Figure of (00.2) Planes of CdS, Molybdenum Substrate Side, Normal to Substrate at Center of Figure.

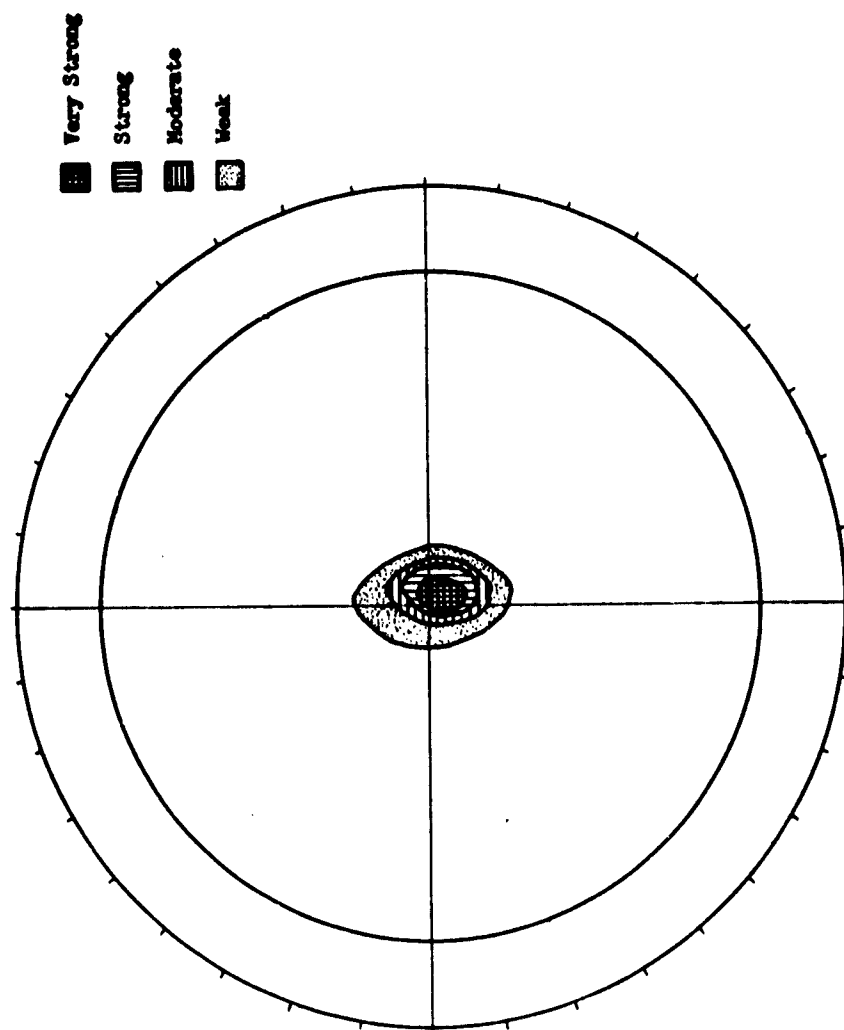


Figure 19: Pole Figure of (00.2) Planes of CoS, Surface Side, Normal to Molybdenum Substrate at Center of Figure.

This has been carried out on two front wall cells, the first being shown in Figure 20, where the illuminant is sea level sunlight. The integrated current is 4.9 ma/cm^2 , while the value measured in sunlight is 5.3 ma/cm^2 . The agreement is quite good. Figure 21 shows the calculations for the same cell in extra-terrestrial sunlight, where the current calculates to be 7.25 ma/cm^2 , representing an increase of 51%, which can be attributed to the higher response at the shorter wavelengths. It is to be noted here that this cell showed very little enhancement effect in measurement of response to monochromatic light with added bias light. Consequently, it probably approaches a linear system (like a p-n junction cell) where the output can be formed from a linear combination of its separate components.

A second cell (339 MN) has been investigated by the same process, with the calculated data shown in Figure 22, for sea level sunlight. The current calculates to 4.25 ma/cm^2 , where the measured current is 6.9 ma/cm^2 , or 62.5% more than calculated. Figure 23 shows the results of spectral response measurements for monochromatic light with and without bias light. As can be seen, a sizeable enhancement effect exists and this is in the direction indicating that sunlight generated current will be higher than the integrated monochromatic response shows. A quantitative evaluation of the effect of enhancement in a cell is not possible at this time.

Considerably more work has been done measuring cell response to two monochromatic beams, pursuing the anomalously high quantum yield to determine its origin. At this time, however, the data is quite incomplete. What is required to present the entire picture is the cell short circuit current as a function of the energies of the photons of each beam and as a function of the photon fluxes of each beam. The observed behavior of the cell in this respect is described as follows:

- 1) For light of the same spectral distribution, short circuit current is proportional to intensity.
- 2) For two incident monochromatic beams, the short circuit current in general is a non-linear function of the intensity of either beam.
- 3) The nature of the non-linear behavior changes with the intensities of the two beams.
- 4) A single crystal rear wall cell has been measured to give 15 electrons per added 2.3 ev photon with bias light photons of 1.35 ev. The overall quantum yield in this case was about 1 electron per 50 photons.

Quantitative data beyond this stage is not complete and it is difficult to draw any valid conclusions.

A number of experiments designed to characterize the electrical and optical nature of the CdS barrier are tentatively scheduled for the coming period. Careful analysis of absorption and photovoltaic response spectra should give a fair description of the important energy levels associated with the barrier. Analysis of the I-V characteristics under monochromatic illumination may lead to a model that can explain the enhancement quantum yield mentioned above.

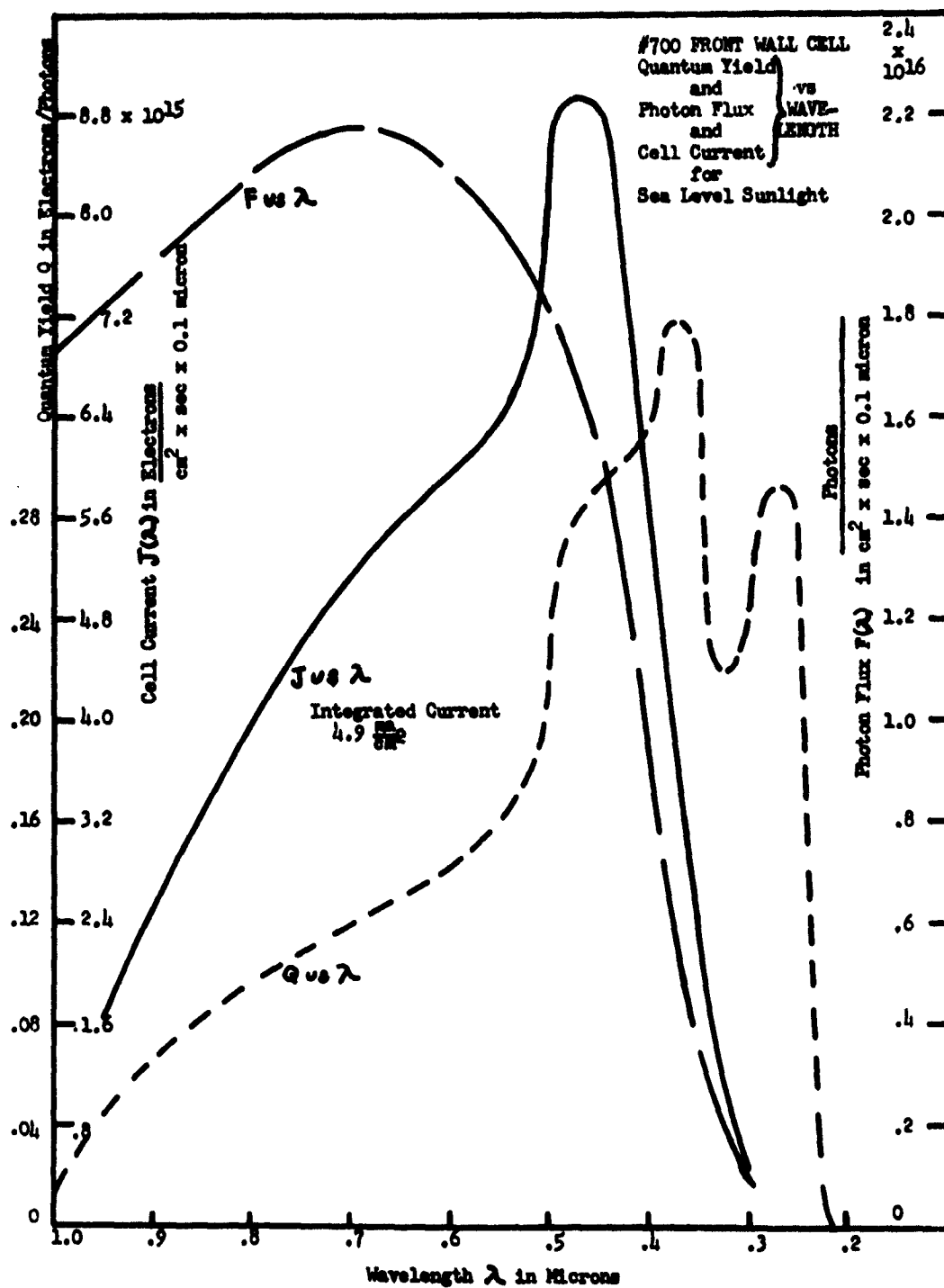


Figure 20

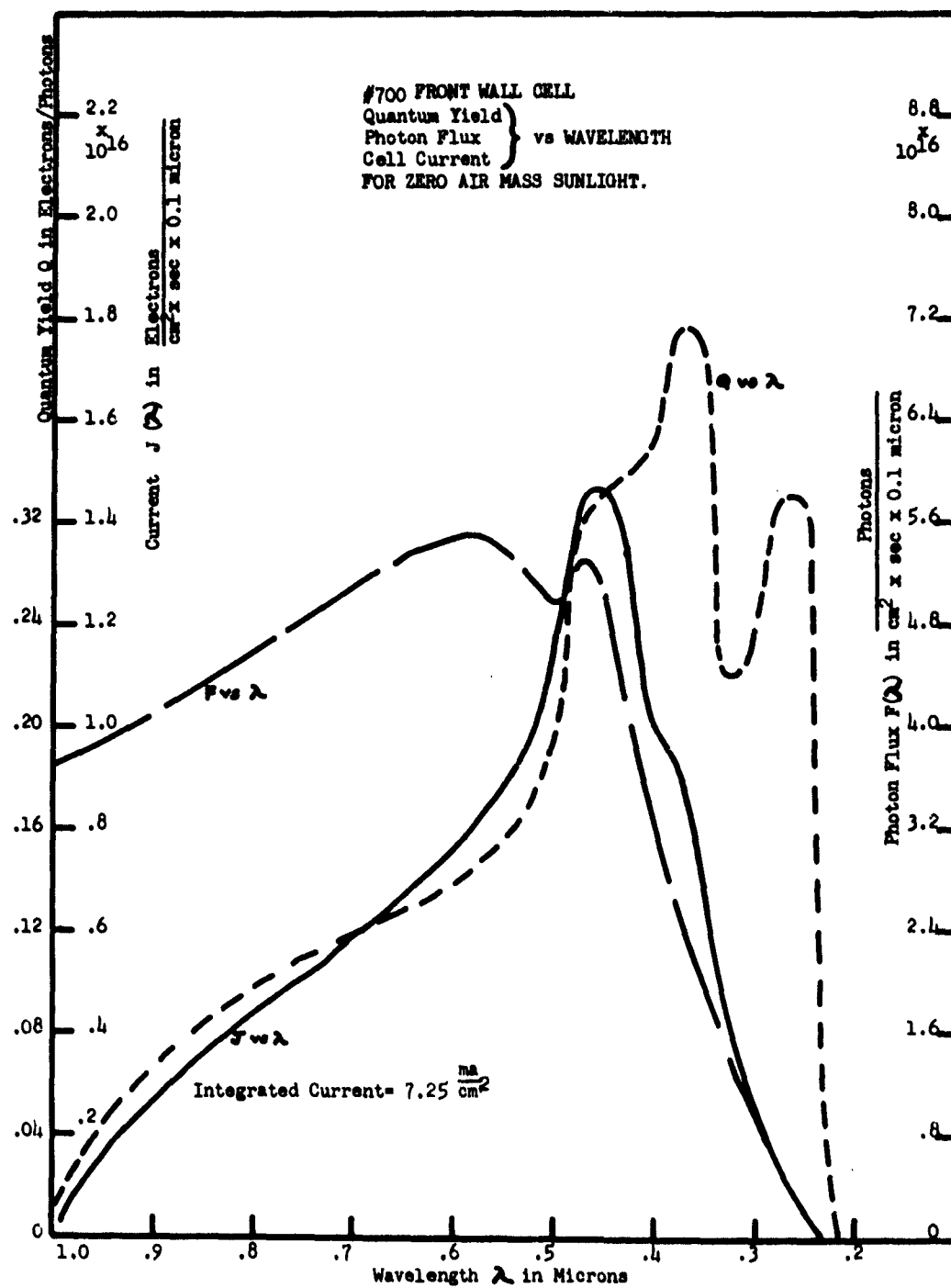


Figure 21

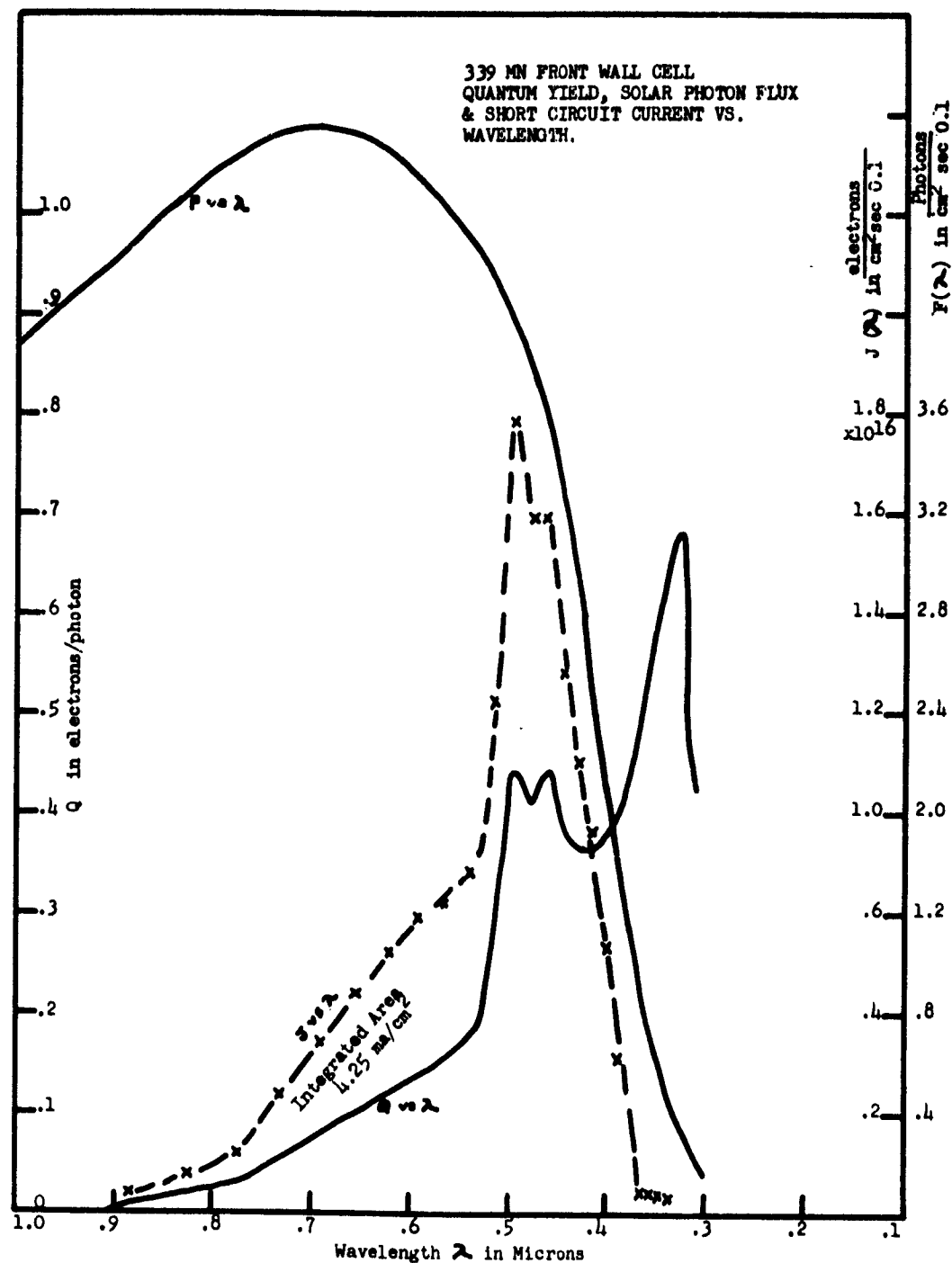


Figure 22

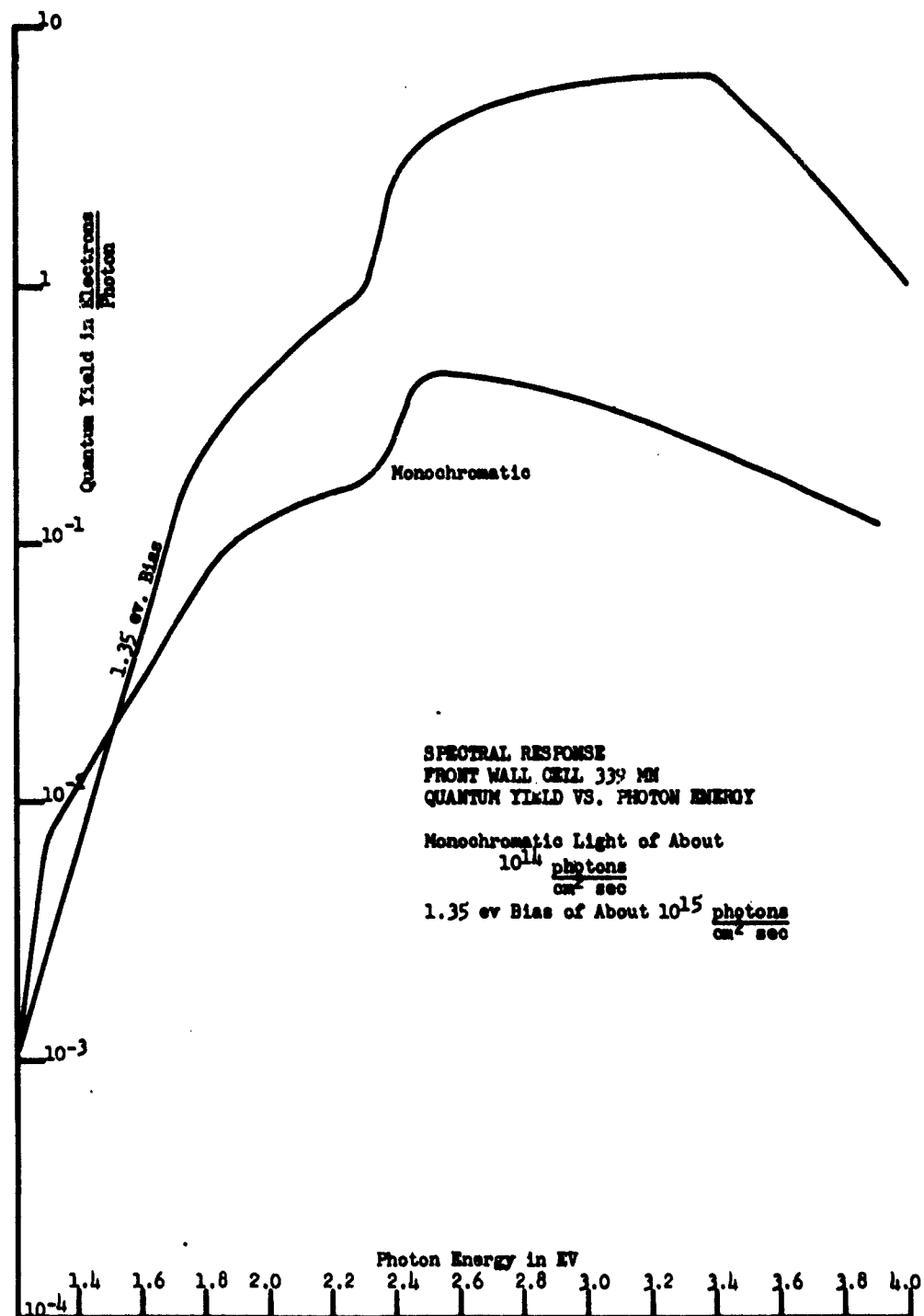


Figure 23

WORK PLANNED FOR NEXT QUARTER

A large number of cells will be fabricated and contacted with various grid materials to statistically evaluate their effectiveness as collector grids.

Experiments with plastics and lamination of cells will continue, with consideration to large area panel designs. No further work on orbital evaluation is planned until after the actual orbital test.

Electrophoretic deposition on molybdenum substrates and sintering experiments will continue.

More emphasis will be placed on life tests and the inhibition of efficiency decay studies.

Efforts to further zone-refine cadmium will be continued using very dry hydrogen, oxygen-free to prevent oxide formation. CdS will also be formed by reacting Cd directly with H_2S .

The Cd distillation apparatus will also be completed, tested and operated in another phase of the high purity CdS experiments.

The microscope light figure apparatus should be completely assembled during the next report period. Plans call for the investigation of grain orientation studies of grain grown CdS films deposited on different types of substrates. Emphasis will be placed on the examination of films deposited on molybdenum substrates.

Further work on etching, especially the high temperature vacuum etching, is planned. Examination of "feed pile" crystals will also be undertaken to determine more precisely the growth habit of these crystals. Comparison between chemically etched, grown, and vacuum etched crystals, and theoretically derived growth forms will be continued. An attempt to correlate this etching data with theoretically derived reaction kinetic equations will be continued.

Attempts will also be made to further improve and control the growth of grains of CdS films.

At the present, only two films of CdS have been examined by pole figure techniques. It is planned that several more films be examined to corroborate the principal results and re-examine the data and technique utilized. A pole figure apparatus for use with the Norelco diffractometer has been constructed, which should provide a greater measure of accuracy for intensity data. Furthermore, the ease and rapidity of data collection will be simplified.

X-ray procedures and apparatus have been developed for dislocation studies in single crystals by means of the Lang technique⁽³⁾. Therefore, a preliminary survey will be attempted on CdS single crystals to determine applicability to perfection, dislocation types and content, and other information on structure.

A number of experiments designed to characterize the electrical and optical nature of the CdS barrier are tentatively scheduled for the next quarter. Careful analysis of absorption and photovoltaic response spectra will give a fair description of the important energy levels associated with the barrier. Analysis of the I-V characteristics under monochromatic illumination may lead to a model that can explain the enhanced quantum yield theory discussed in the text.

LIST OF REFERENCES

- (1) F. A. Shirland, J. C. Schaefer, G. A. Wolff, E. R. Hill, First Quarterly Progress Report, Contract AF 33(657)-9975, Pages: 7, 12, and 16.
- (2) D. C. Reynolds and L. C. Green, "Growth and Properties of Cadmium Sulfide Crystals", Solid State Physics in Electronics and Telecommunications, 2, Academic Press, 1960, Page: 859.
- (3) A. R. Lang, Journal of Applied Physics, 30, Page: 1748, 1959.

CRYSTAL MORPHOLOGY IN EVAPORATION, EQUILIBRIUM AND GROWTH IN THE VAPOR PHASE

G. A. Wolff and J. R. Hietanen
Harshaw Chemical Company
Cleveland 15, Ohio

The morphology of crystals in evaporation and condensation processes can be derived from surface energy calculations which also lead to periodic bond chain (PBC) - vectors. These vectors are the unit vectors of strong bond chains. It is found that in crystal growth (condensation) the crystal edges of the growth form are parallel to such bond chains while in solution (evaporation) the ridges of the solution form are parallel to them. Differences between derived and observed condensation or evaporation morphology lead to important conclusions concerning the atomic structure of the crystal surface. The influence of dislocations, polytypisms, degree of ionicity and covalency, and the lack of a center of symmetry on the condensation and evaporation habit of crystals is discussed. The application of the optical reflection (light figure) method as a research tool to investigate the mechanism of evaporation and condensation of crystals is described. Example equations are derived for materials which dissociate upon evaporation.

CRYSTAL MORPHOLOGY IN EVAPORATION, EQUILIBRIUM AND GROWTH IN THE VAPOR PHASE

By

G. A. Wolff and J. R. Hietanen
Harshaw Chemical Co.
Cleveland 15, Ohio

With the advent of solid state electronics much attention has been placed on the understanding of the structural aspects of solids. For example, crystal imperfections and their effect on the electrical and optical behavior of solid state devices have undergone a great deal of investigation. Many tools, such as mass spectrometry and x-ray diffraction, have been used with much success to bring forth useful data. The surface morphology of crystals has, however, hardly been investigated and only superficially as far as the interpretation of the bonding and kinetical aspects of crystal surfaces are concerned. Ways in which such an investigation can be pursued will be described.

There are three types of planes that enclose a crystalline body during any stage of its morphological development. They are designated as F-, S-, and K-planes; i. e. flat-, stepped-, and kinked- planes. Their relation to one another is illustrated in Table I.

The crystal forms that these planes enclose and the relation of the various form types is given in Table II.

The critical interpretation of crystal forms and their relation to equilibrium, crystal growth, and solution kinetics supplies important information on the bond structure and the kinetical aspects of crystal surfaces. In this interpretation the following facts appear to be of importance:

- 1) An equilibrium form of a crystal is bounded by only F- planes. The edges as interceptions of the existing F-planes are all parallel to bond chains (strong bond arrays). This holds true for any type of bonding.
- 2) For growth or dissolution processes, where heat or material diffusion is not rate controlling, a crystal growth form or an etch pit solution form is finally bounded by only F-planes. Such forms are the result of what from a crystallographic point of view is called a preferential growth or dissolution process.
- 3) The presence of screw dislocations gives rise to vicinal planes. These dislocations do not affect the strength or direction of the strong bonding arrays. The kinetics of evaporation and condensation are, therefore, still greatly determined by these bonding arrays. In kinetic or equilibrium studies of this type, the presence of dislocations are actually quite helpful since they provide surface depressions (pits) and elevations (hillocks) which provide readily available sites at which evaporation or condensation can be initiated.

The light-figure technique⁽¹⁾ has proved to be quite useful in the

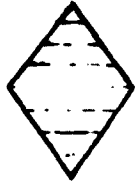
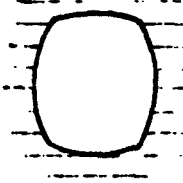

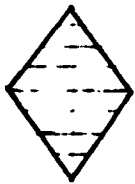
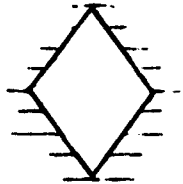
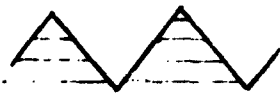

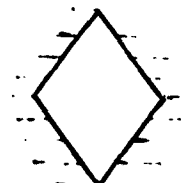

TABLE I

<u>Type of Plane</u>	<u>Surface Atom Bonding Energy</u>	<u>Number of PBC Vectors</u>
F-plane	$\xi_{\frac{1}{2}} + S\phi_1, S \gg 2$	Two or more
S-plane	$\xi_{\frac{1}{2}} + \phi_1$	one
K-plane	$\xi_{\frac{1}{2}}$	none

$\xi_{\frac{1}{2}}$ represents the bonding energy of the atom, molecule, ion, etc. in the equilibrium or "half-crystal" position. ϕ_1 represents the bonding energy of first nearest neighbors. PBC vectors are periodic bond chains that exist in a crystal face. All atoms, molecules, ions, etc. of a PBC vector are bonded to the crystal by one bond more than the atom in the equilibrium position.

TABLE II

(Schematic, Idealized)

Process	Starting Form	End Form		
		Crystal Positive	Crystal Negative (Void)	Cry. Pos. & Neg.
Condensation (Growth)	Any form of Positive or Neg. (void) Crystal	Growth Form (Polyhedron) 	Negative Solution Form (Rounded Void) 	Form Hillocks and Etch Pits 
Equilibrium (Equilibration)	Any	Equilibrium Form (Polyhedron) 	Equilibrium Form (Polyhedron) 	
Evaporation	Any	Solution Form (Rounded body with curved ridges intersecting at more or less sharp points.) 	Negative Growth Form (Polyhedron) 	

The growth, equilibrium, and negative growth forms have PBC vectors parallel to the edges. These forms are enclosed by P -planes (S - P -planes can persist in some instances). The solution and negative solution forms have PBC vectors parallel to the curved ridges. These forms are enclosed by vicinal K -planes.

investigation of growth and dissolution forms. By this technique one is able to determine the direction of steps on the crystal surface of dimensions smaller than the wave length of light and thus elucidate the directions of the strong bonding arrays. As a result, important crystallographic aspects of crystal surfaces can in many cases be uncovered which remain obscure during optical or electron microscope studies. Further, the pattern observed during a light-figure investigation can be directly related to the stereographic pattern of a theoretical growth form. Fundamental conclusions, can, therefore, be made regarding the structural bonding of surface atoms, ions, molecules, etc. Table III depicts this relationship.

This type of study has been applied to the crystals of the diamond type structure⁽²⁾. Morphology studies of growth and solution forms of these structures has revealed that (001) and (111) are the stable planes on diamond while (001), (111) and (113) appear on germanium, silicon and gray tin. See (A) and (C) of Figure 1. Theoretical equilibrium form calculations taking into account first and second nearest neighbor interactions account for the appearance of (111) and (001), respectively, on these structures but the appearance of (113) could be accounted for only after a surface deformation was assumed in which surface atoms moved one quarter of the lattice body diagonal into energetically more favorable positions. Surface deformation could also, in fact, explain the appearance of (001) and second nearest neighbor interactions (which are in reality quite small) could thus be disregarded. H. E. Farnsworth⁽³⁾ has verified the surface deformation in this plane. The morphology of α -SiC (of sphalerite structure) reported by N. W. Thibault⁽⁴⁾ reveals the presence of (113) but not of (113). See (B) of Figure 1. A study of this structure reveals that the two antipode planes (113) and ($\bar{1}\bar{1}\bar{3}$) can be composed entirely of atoms of the opposite type, i. e. Si and C. The existence of (113) can, therefore, be attributed to the rearrangement of silicon atoms at the surface while the absence of ($\bar{1}\bar{1}\bar{3}$) can be related to the absence of surface deformation in diamond.

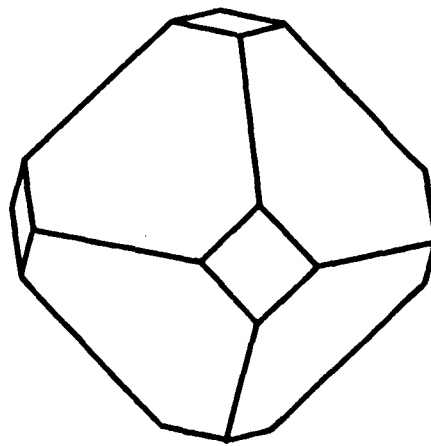
This type of study has also been applied to other polytypes of SiC⁽⁵⁾. Good agreement has been observed between theoretically calculated and observed forms. Figures (2) and (3) are the stereographic projections for the theoretically calculated equilibrium forms of all polytypes. Table IV lists the planes, as a function of bonding conditions, that enclose the equilibrium forms. Table V⁽⁶⁾ gives a comparison between observed and calculated planes for many of the polytypes.

It is interesting to note that all the polytypes can be compared to a single set of calculated equilibrium forms. In this comparison the sphalerite type lattice can be taken as the basic lattice. The polytypes can then be considered to consist of this basic lattice with systematically spaced "twinning" or stacking on the (111) plane. Close examination of the pyramidal and prismatic planes on equilibrium forms shows that these planes can be composed of (111) and (001) planes in the sphalerite type structures on either side of a stacking fault. In an analogous manner to the α -SiC mentioned above, the existence of composed planes containing (113) as one of the planes has been proposed. The planes that result by a combination of (111) and (113), with due regard to modifications introduced at the stacking faults, have been calculated and are given in Table VI. These planes have been included in Table V.

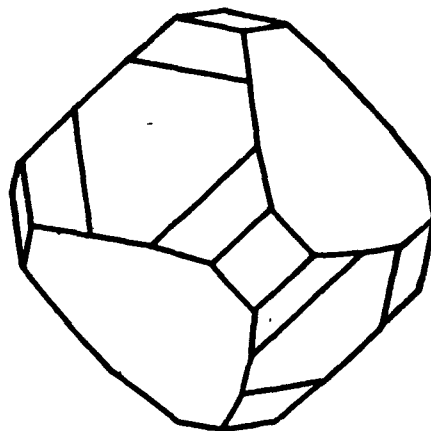
The difference in behavior of germanium surfaces when thermally etched in oxygen and in chlorine can also be understood by micromorphology studies⁽⁷⁾.

TABLE III

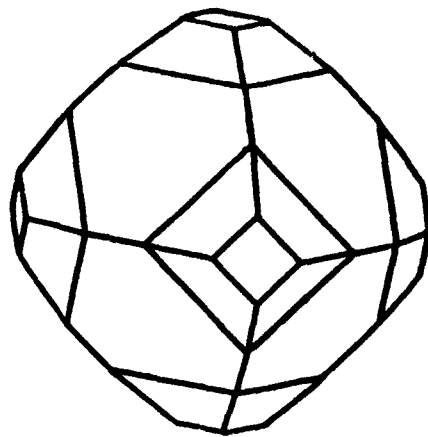
<u>Feature</u>	<u>Light-Figure</u>	<u>Stereographic Projection</u>
Spot or point of intersection of lines.	Represents F-planes whose dimensions are greater than the wavelength of light.	Represents a stable plane.
Lines ending in or crossing other lines at intersections.	Represent microscopic planes (vicinal S-planes) tilted in only one zonal direction. They are made up of steps composed of two F planes of microscopic dimensions. The step distances are of dimensions comparable or smaller than the wavelength of light applied.	Represents edges between two planes.



A



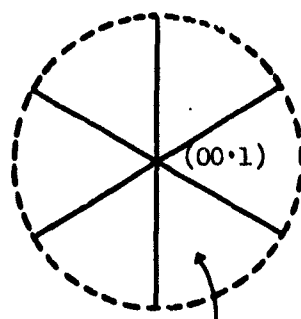
B



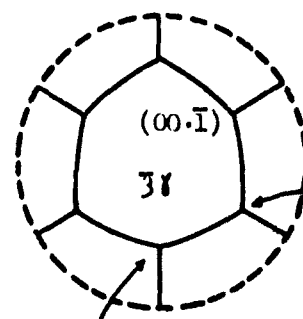
C

Figure 1. - Common Habits of (a) diamond (111), (112), (113), and (001); (b) β -silicon carbide (111), (112), (113), and (001); and (c) silicon, germanium, or gray tin (111), (112), (113), and (001).

$$\gamma \leq 1/3$$



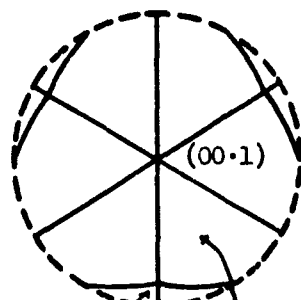
$$4/3 \gamma (2M+N) \cdot 4/3 \gamma (M+2N) \cdot 1$$



$$(10 \cdot 1/3(2M+N))$$

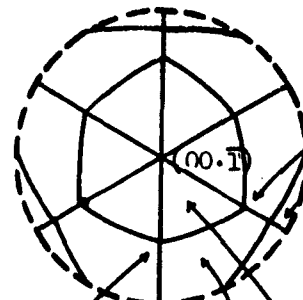
$$(01 \cdot 1/3(M+2N))$$

$$1/3 \leq \gamma < 1$$



$$(10 \cdot 1/3(M-N))$$

$$1/3 [(3-\gamma)M + 4\gamma N] \cdot 1/3 [(3-\gamma)N + 4\gamma M] \cdot \gamma$$



$$(10 \cdot 1/3(2M+N))$$

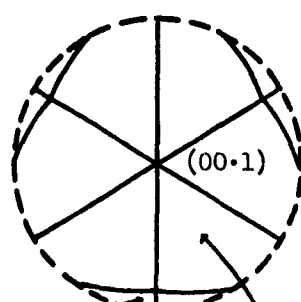
$$1/3(2M+N)(3\gamma-1) \cdot 1/3(M+2N)(3\gamma-1) \cdot \bar{1}$$

$$1/3(2M+N)(\gamma+1) \cdot 1/3(M+2N)(\gamma+1) \cdot (1-2\gamma)$$

$$(01 \cdot 1/3(M+2N))$$

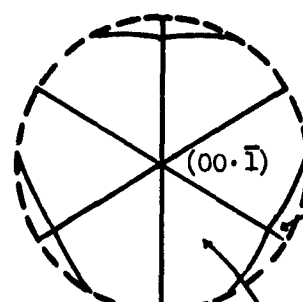
$$(01 \cdot 1/3(M-N))$$

$$\gamma = 1$$



$$(10 \cdot 1/3(M-N))$$

$$2/3(M+2N) \cdot 2/3(2M+N) \cdot 1$$



$$2/3(2M+N) \cdot 2/3(M+2N) \cdot \bar{1}$$

$$(01 \cdot 1/3(M-N))$$

Figure 2 - Polytype Equilibrium forms for various ratios of cation to anion bonding. These are stereographic projections of general polytype equilibrium form where γ = cation (C) to anion (A) contribution to surface energy. Surface energy is given by $\sigma_{hkl} = \frac{(U_h + V_k + W_l)A}{\text{unit area}}$ where U·V·W are given

as indicated in the figure. M and N refer to sum of first and second Zhdanov notations, respectively, for all polytypes. In the 15R polytype, for example, the Zhdanov notation is 32 32 32. M=9 and N=6.

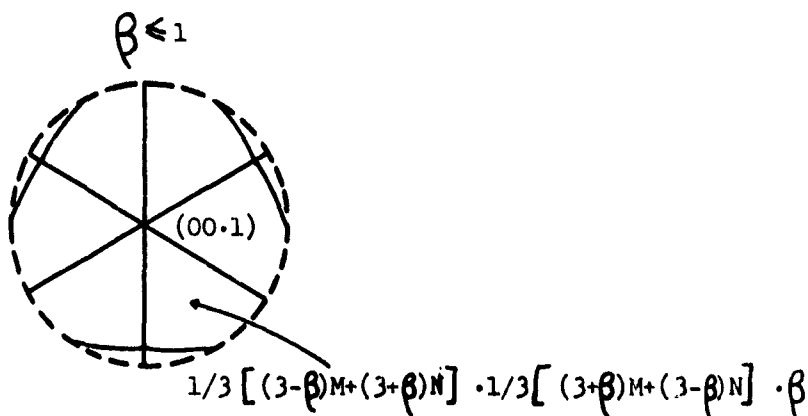
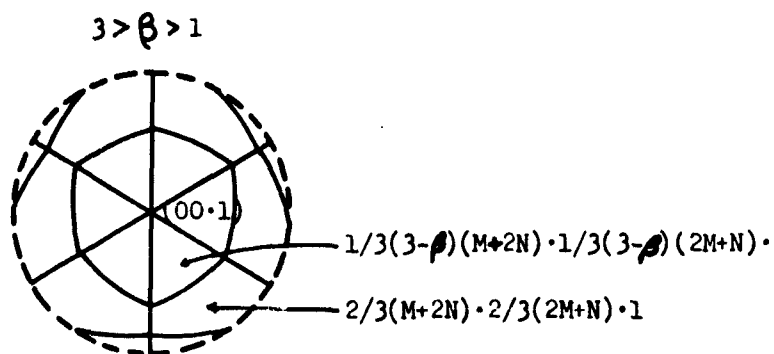
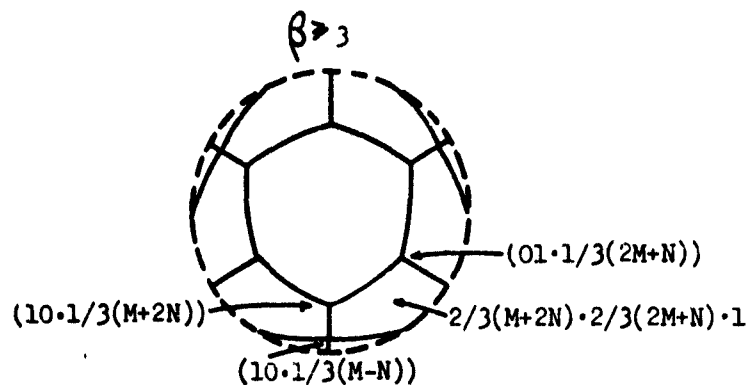


Figure 3- General Polytype Equilibrium forms for Various Ratios of c-directional to a-directional bonding. These are stereographic projections of general polytype equilibrium forms for varying ratio of c-directional to a-directional bonding strength contribution to the surface energy. β equals c-directional to a-directional ratio. Surface energy is given by $\sigma_{hkl} = \frac{(U_h + V_k + W_l)a}{\text{unit area}}$ where U·V·W are given as indicated in the figure. M and N have same meaning as denoted in Figure 2.

TABLE IV

	$\delta \geq 3$	$3 > \delta > 1$	$\delta = 1$	$1 > \delta > 1/3$	$\delta \leq 1/3$	$\beta \geq 3$	$3 > \beta > 1$	$\beta \leq 1$
$0.1/3(M+2N)$	x	x				x	x	
$1.1/3(2M+N)$	x	x				x	x	
00.1	x	x	x	x			x	x
$0.1/3(M-N)$		x	x	x		x	x	x
$01.1/3(M-N)$		x	x	x		x	x	x
00.1		x	x	x	x		x	x
$01.1/3(M+2N)$				x	x	x	x	
$10.1/3(2M+N)$				x	x	x	x	

M and N are as denoted in Figure 2. δ is the ratio of cation to anion dangling bond energy contribution to the surface energy. β is the c-directional to a-directional contribution to the surface energy. X indicates the plane that appears on the equilibrium form under the condition imposed at the top of each column of the table.

TABLE V

	a	a	b	a	c	a	b	a	d	b	b	b
	4H	6H	8H	15R	19M	21R	27R	33R	51Ra	75R	84R	87R
0001	2	67	2	22	2	2	2	1		2	2	2
01. $1/3$ (2M+N)	11	56		13	1	4		5	5	3	1	2
10. $1/3$ (M+2N)				8	2	3	1	6	5	1	2	4
10. $1/3$ (M-N)	5	26		9		3	1	3	5		2	1
01. $1/3$ (M+N) $+ \frac{m_0}{2}$	8	34	1		2	1		4	5			2
10. $1/3$ (M+N) $+ \frac{n_0}{2}$					1	2	1	5	5	3		3
10. $1/3$ (M+5N)				1								
01. $1/3$ (5M+N)						1						
10. $1/3$ (M+5N)-p	5	23		2		1			2			
01. $1/3$ (5M+N)-p				1	3				5			
10. $1/3$ (M+2N)-p				2		1		2	4	1		
01. $1/3$ (2M+N)-p		17	3	5		1		2	4	1	1	
11. $1/3$ (M+N)	5	5		5								

A comparison between observed and calculated planes. The table includes only those polytypes where morphology data was available. The numerical values given are the number of times the respective planes were observed. Lower case letters denote references. M and N are as denoted in Figure 2. n_0 is the number of odd n's appearing in Zhdanov's notation. m_0 is the number of odd m's appearing in Zhdanov's notation. p is the number of mn combinations in Zhdanov's notation.

TABLE VI

$10 \cdot 1/3(M+N/2) + 1/2n_0$	$01 \cdot \overline{1/3(M+N/2) + s/2n_0}$
$01 \cdot 1/3(N+N/2) + 1/2m_0$	$10 \cdot \overline{1/3(N+N/2) + 1/2m_0}$
$10 \cdot 1/3(M+5N)$	$01 \cdot \overline{1/3(M+5N)}$
$01 \cdot 1/3(5M+N)$	$10 \cdot \overline{1/3(5M+N)}$
$10 \cdot 1/3(M+5N) - p$	$01 \cdot \overline{1/3(M+5N) - p}$
$01 \cdot 1/3(5M+N) - p$	$10 \cdot \overline{1/3(5M+N) - p}$
$10 \cdot 1/3(M+2N) - p$	$01 \cdot \overline{1/3(M+2N) - p}$
$01 \cdot 1/3(2M+N) - p$	$10 \cdot \overline{1/3(2M+N) - p}$
$11 \cdot \overline{1/3(M+N)}$	$11 \cdot 1/2(M+N)$

Calculated equilibrium form planes resulting from surface deformation and/or foreign atom absorption. M and N are as denoted in Figure 2. n_0 is the number of odd n's appearing in Zhdanov's notation. m_0 is the number of odd m's appearing in Zhdanov's notation. p is the number of mn combinations in Zhdanov's notation.

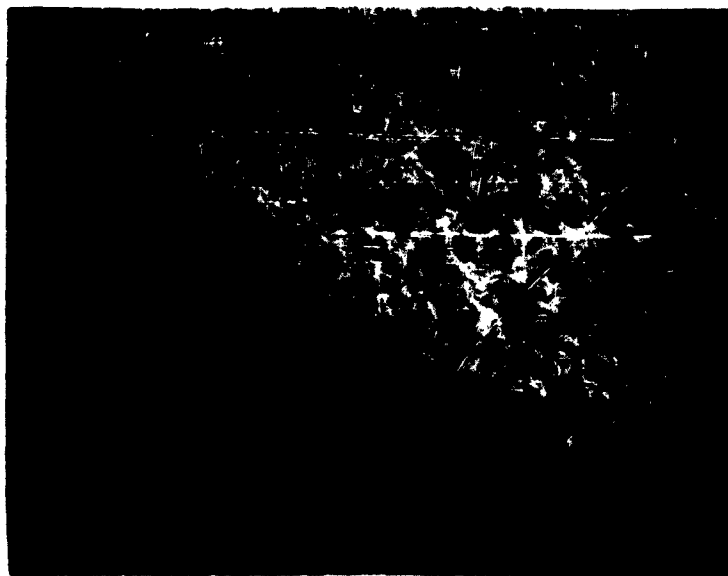
Figure (4) shows two photomicrographs of a germanium (111) plane. The sample was cracked and one piece etched in chlorine and the other in oxygen. (The piece with the larger pits was etched in oxygen). Although the etch pit shape as observed in the photomicrographs can be evaluated (the walls of the pits being rotated 60° in the two cases), it is rather difficult to make definite conclusions regarding the stability of certain bonding arrays. The light-figure patterns of these surfaces reveal, however, a clear three-fold symmetry. The complete light-figure patterns for germanium etched in these gases are shown in Figure (5) and (6). Included is the theoretical etch pit (negative growth) form that appears on various surfaces of a hypothetical germanium crystal. Among the conclusions to be drawn from this comparison is that the chlorine leaves either the surface unchanged and no absorption or atomic rearrangement has taken place; or the univalent chlorine singly binds to the dangling bonds of the germanium surface atoms. This follows from the good match observed between the chlorine light-figure and the theoretically calculated germanium equilibrium form where only first nearest neighbor interactions were considered. Oxygen etching, however, results in the formation of new stable bonding arrays. This is understood by the appearance of (001) and $[1\bar{1}0]$ zone between the planes (111) and (111).

The light-figure reflection patterns of some vapor etched materials of wurtzite and/or sphalerite structure are shown in Figure (7). Similarity between these forms and the theoretically calculated forms is evident. The ZnS pattern, for example, exhibits a great deal of similarity with the theoretically calculated habit for the case $3 > \delta > 1$ or $1 > \delta > 1/3$, depending on crystal polarity, in Figure (8). The reason for the appearance of (11.0) has yet to be determined. The CdS patterns also reveal some similarity with this case although two additional planes are seen to appear. Similar statements hold for the other patterns. A comparison of the observed and calculated forms suggests that just a little more experimental data are necessary to provide for a complete interpretation. The decrease in the complexity of the evaporation pattern of various materials (1) with the change from sulfides via selenides to tellurides and (2) with the anions constant, e.g., in the change from CdS to ZnS, suggests the need for vapor and vacuum etching experiments at various temperatures. The indication is that although at the evaporation temperatures of CdS, for example, only Cd and S_2 is formed in the vapor phase this is not so at the surface where the appearance of (10.3) implies the formation of larger molecules such as S_4 , S_6 and S_8 . The difference in evaporation and growth forms on CdS lends further support to this hypothesis. There is also a need for some restrictive assumptions in the equilibrium form calculations. These might include, for example, surface deformation and foreign atom absorption.

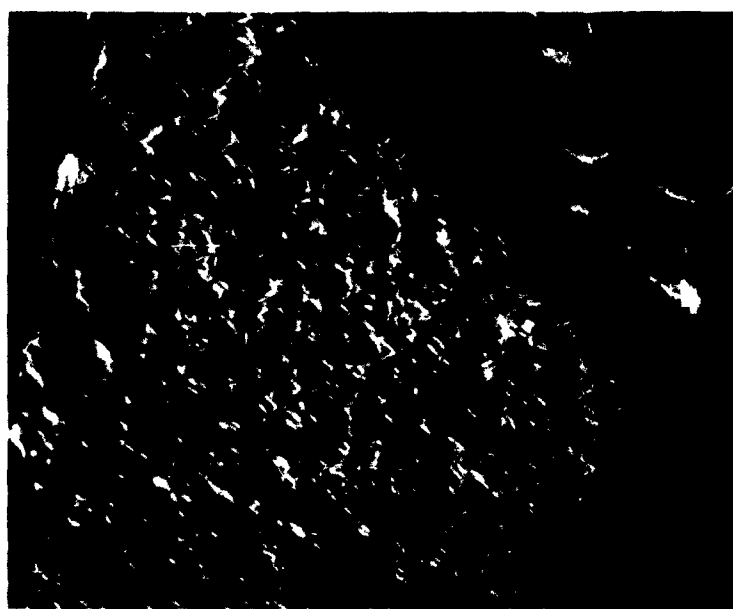
The possibility of the formation of long sulfur chains or rings on CdS during an evaporation process implies the need for a careful evaluation of the kinetic aspects of evaporation and condensation. The effects of the kinetics of these two processes on the condensation coefficient α needs, in particular, to be better understood. G. A. Somorjai⁽⁸⁾⁽⁹⁾ has recently dealt with this problem.

For demonstration purposes the following possible examples of evaporation are suggested:

- 1) CdS could break away from a kink site (1) and diffuse onto the crystal



(a)



(b)

Figure 4. - Photomicrographs of Ge sample etched in Cl_2 and O_2 . Larger etch pits is that piece of the sample which was etched in O_2 . (a) 70x, (b) 270x.

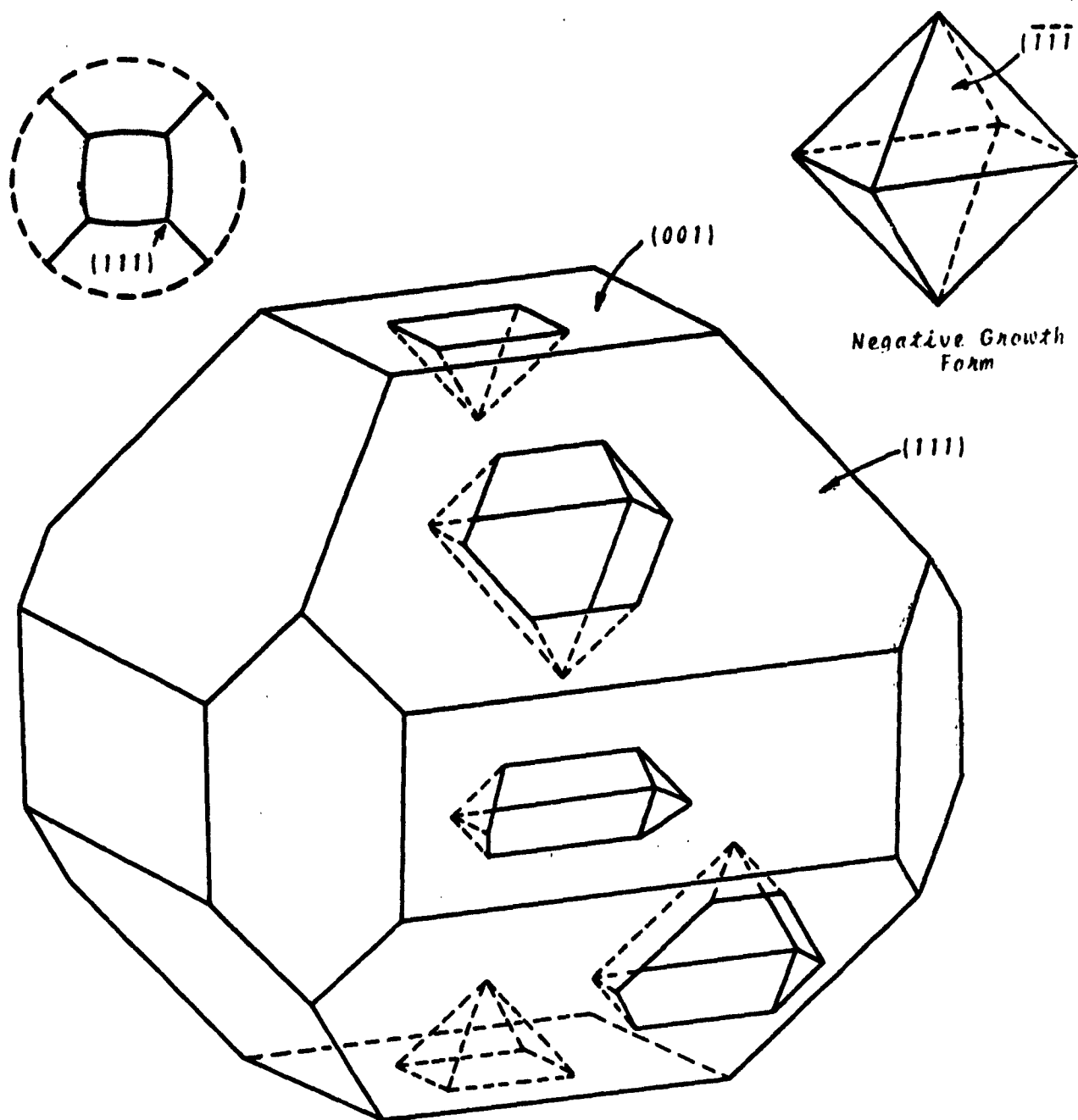


Figure 5. - The stereogram corresponds to the light-figure pattern observed on a chlorine etched germanium sample. This stereogram also corresponds to the theoretical equilibrium form when only first nearest neighbor interactions are considered. The negative growth form is included. The intersection of this form with various surfaces of a general germanium crystal is given. Only those edges that are PBC vectors are stable. Edges not parallel to PBC vectors are unstable and disappear. In the stereograms lines between points of intersection represent stable PBC vectors. In the case represented here, the resulting etch pit form on (111) would be a triangle.

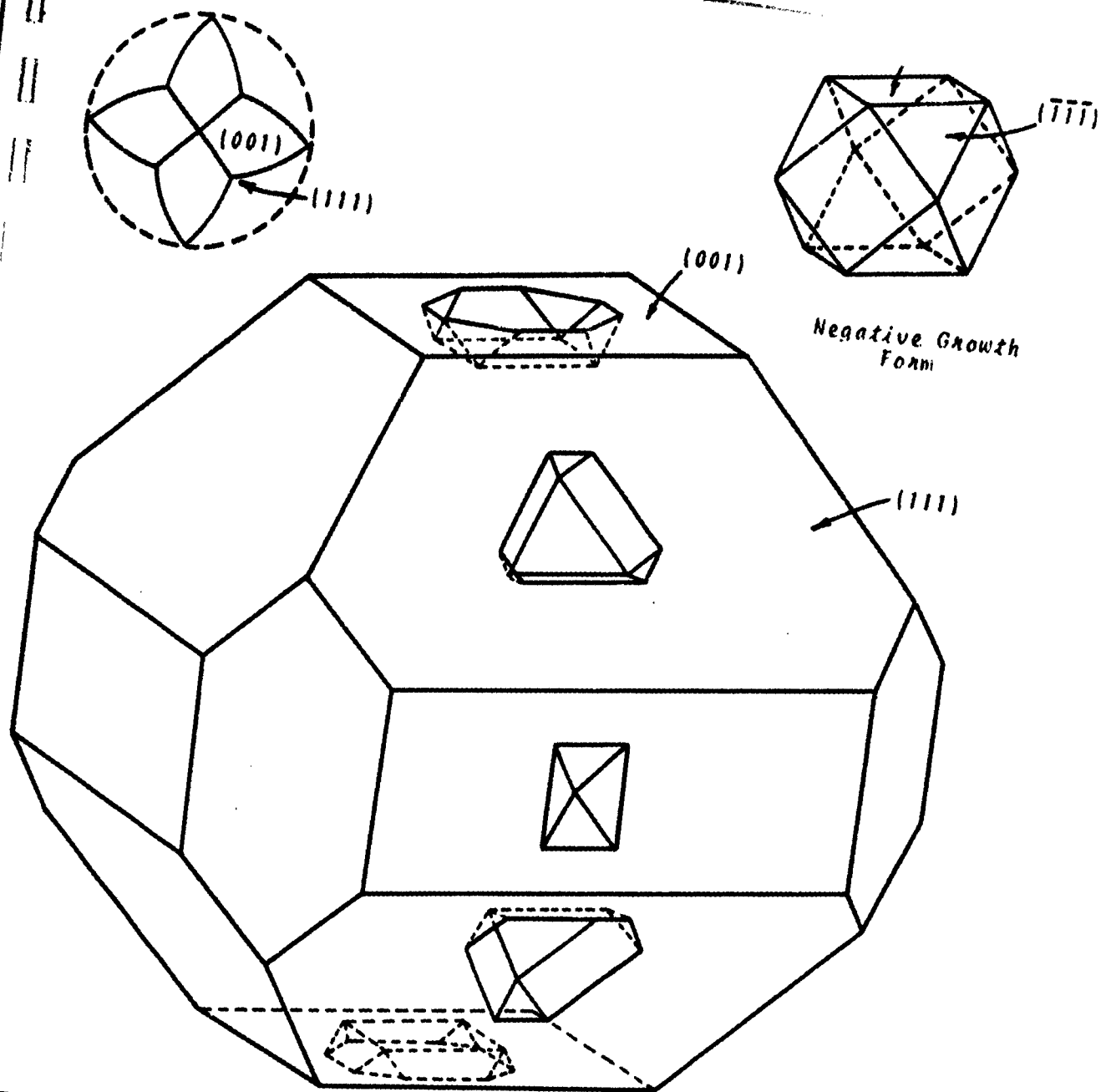


Figure 6. - The stereogram corresponds to the light-figure pattern observed on an oxygen etched germanium sample. This stereogram can be associated with the light figure pattern in the manner suggested in Table III. The positive growth form is omitted. The negative growth form is included. The intersection of this form with various surfaces of a general germanium crystal is given. Only those edges that are PBC vectors are stable. Edges not parallel to PBC vectors are unstable and disappear. In the stereogram lines between points of intersection represent stable PBC vectors. In the case represented here, the resulting etch pit form on (111) would be a triangle rotated 180° to the pit form given in Figure 5.

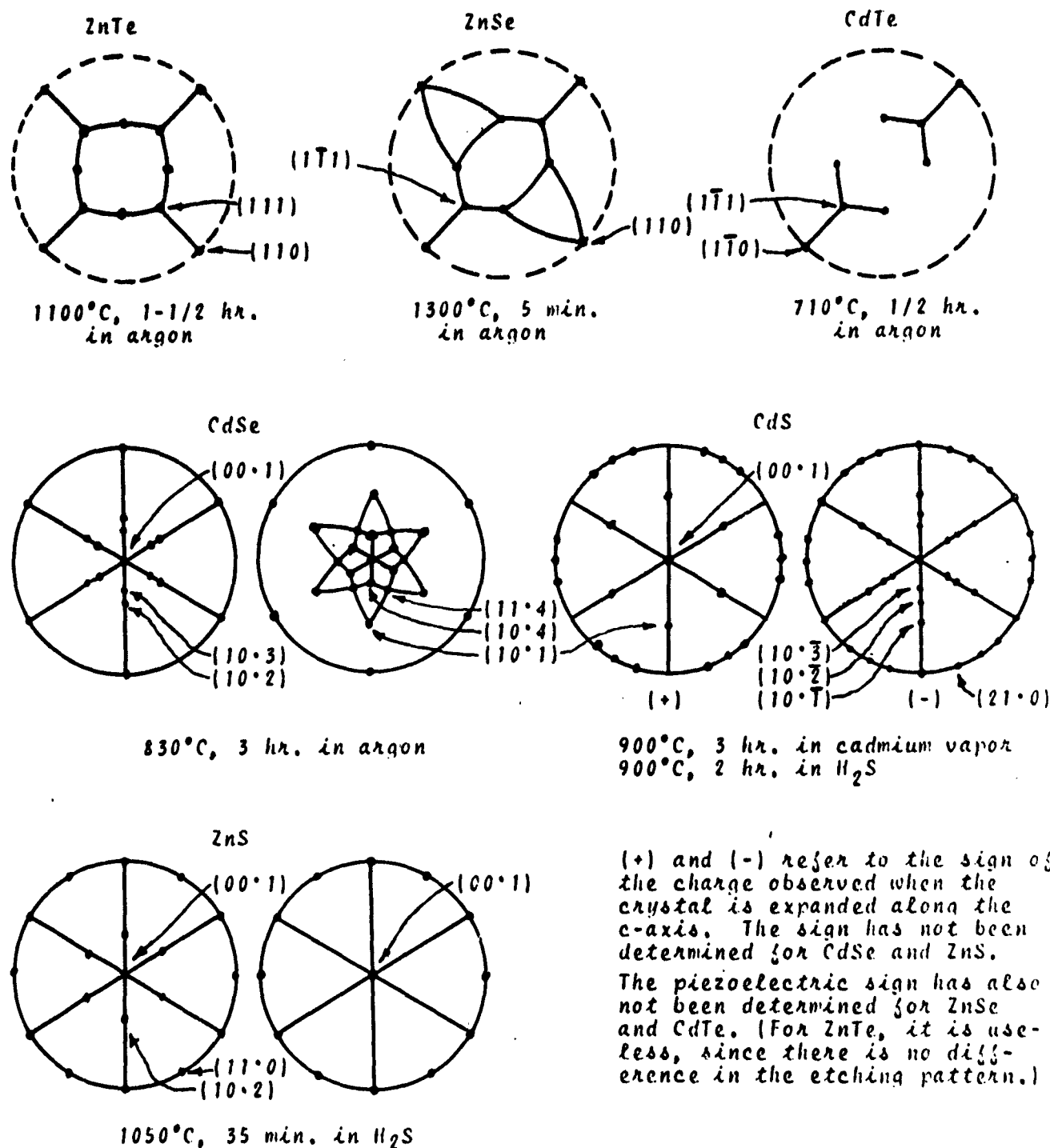
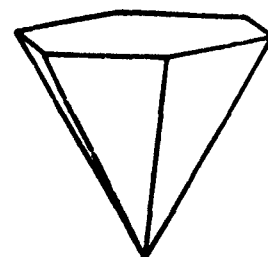
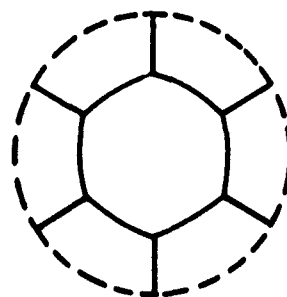
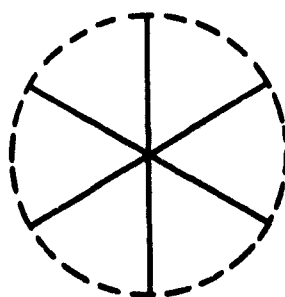
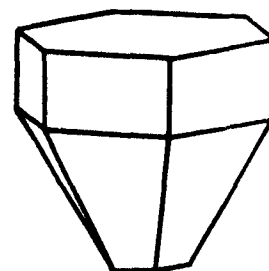
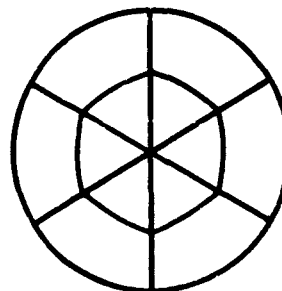
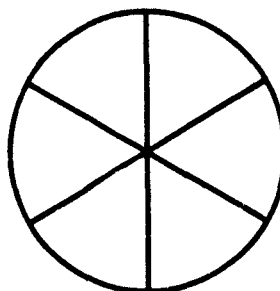


FIGURE 7- STEREOGRAPHIC PROJECTIONS OF WURTZITE AND SPHALERITE TYPE STRUCTURES RESULTING FROM THERMAL AND GAS ETCHING.

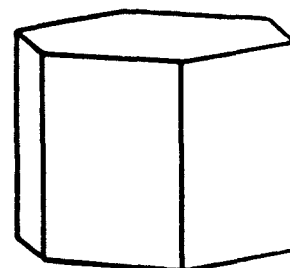
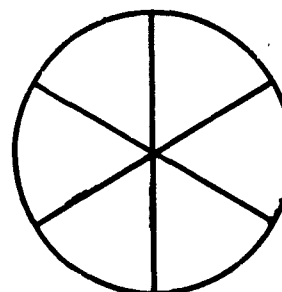
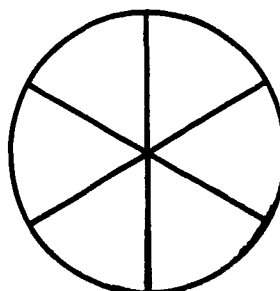
$$\gamma \leq \frac{1}{3}$$



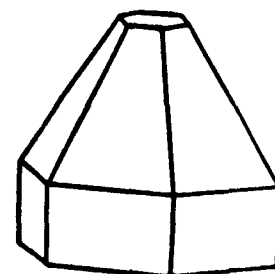
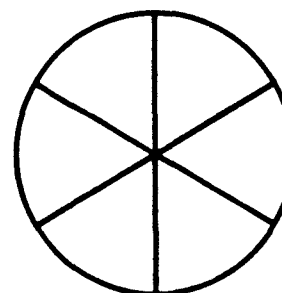
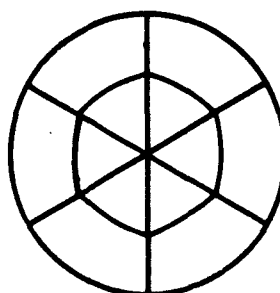
$$1 > \gamma > \frac{1}{3}$$



$$\gamma = 1$$



$$3 > \gamma > 1$$



$$\gamma \geq 3$$

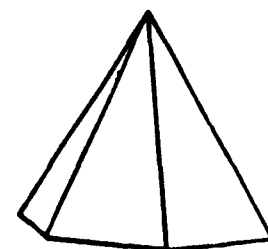
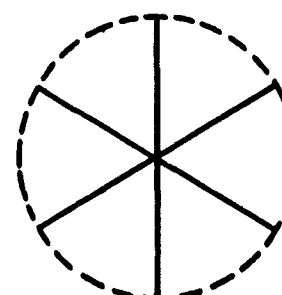
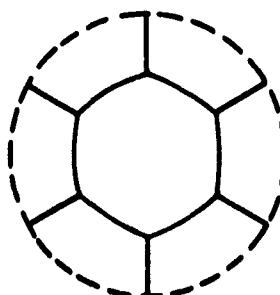
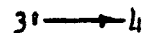


Figure 8. - Theoretically calculated equilibrium forms of wurtsite type materials for varying ratios of cation (C) to anion (A) contribution to the surface energy.

surface (3), break up into 2Cd and S₂, (3') and then evaporate (4). Indices 1, 3, 3' and 4 denote the equilibrium site (1); the surface adsorption site (3) for CdS; (3') for Cd and S; and the vapor phase (4). (This analysis assumes the formation of S₂. The same process considering the formation of S₄, S₆, or S₈ could also be calculated.) In this process the rate controlling step could be the breaking away of CdS from the kink site or the breaking up of 2CdS into 2Cd and S₂. The reaction can be expressed as follows:



$$\left[k_{13} - k_{31}(\text{CdS})_3 \right] C_h = 2 \left[k_{33'}(\text{CdS})_3^2 - k_{3'3}\text{Cd}_3^2\text{S}_3 \right] = \begin{cases} k_{3'4}\text{Cd}_3 - k_{43'}\text{Cd}_4 \\ 2(k_{3'4}\text{S}_3 - k_{43'}\text{S}_4) \end{cases}$$

C_h is the concentration of kink sites on the crystal surface. The solution of this equation under both processes results in cubic equations that have a real and two complex solutions. The mathematics becomes involved and it appears difficult to give a good physical explanation of the results. The problem can be simply solved, however, if the steps preceding and following the rate determining step are considered to occur at a much greater rate than the rate determining step and, as such, assumed to be in quasi-equilibrium. Under the conditions when 3 → 3' is rate determining the following equation results:

$$-\frac{dn}{Adt} = 2k_{3'3} \left(\frac{k_{43'}}{k_{3'4}} \right)^2 \frac{k_{43'}}{k_{3'4}} \left[(\text{Cd}_4^2\text{S}_4)_s - \text{Cd}_4^2\text{S}_4 \right] \quad (1)$$

The sub-s refers to equilibrium (saturation). When 1 → 3 is the rate determining step the following equation results:

$$-\frac{dn}{Adt} = C_h k_{31} \left\{ \frac{k_{3'3}}{k_{33'}} \left(\frac{k_{43'}}{k_{3'4}} \right)^2 \frac{k_{43'}}{k_{3'4}} \left[(\text{Cd}_4^2\text{S}_4)_s - \text{Cd}_4^2\text{S}_4 \right] \right\}^{\frac{1}{2}} \quad (2)$$

Both equations can be compared with the equation:

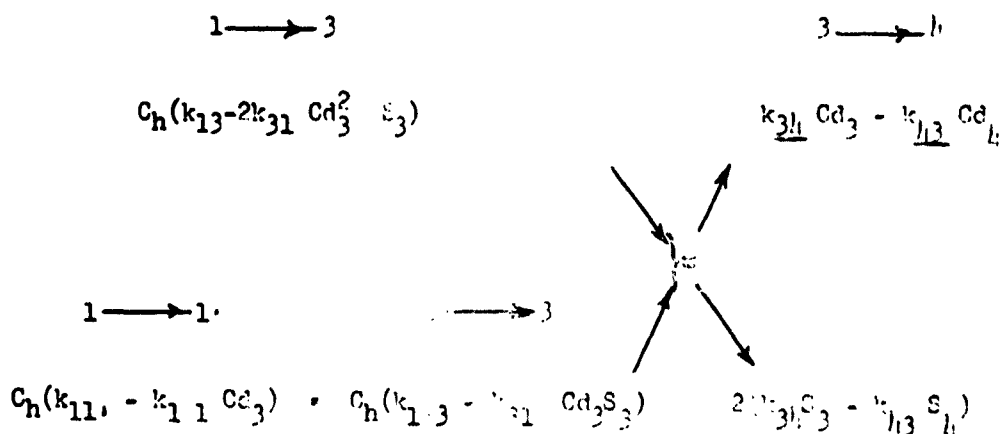
$$-\frac{dn}{Adt} = \alpha \sqrt{\frac{kT}{2\pi m}} (C_{Ls} - C_L)$$

When $k_{43} = \delta \sqrt{\frac{kT}{2\pi m}}$ and the vapor phase composition is kept at the ratio Cd:S=1, then $Cd_L = 2S_L$; $C_L = Cd_L + S_L$ and $(Cd_L^2 S_L) = 4/27 C_L^3$. It follows that $\alpha_1 =$

$$\frac{2k_{3'3}}{k_{3'4}^2 k_{3'4}} \frac{kT}{2\pi} \frac{\delta^2}{m_{Cd} m_{S_2}^2} \frac{1}{27} (C_{Ls}^2 + C_{Ls} C_L + C_L^2) = f(C_L) \text{ for (1).}$$

δ is the cadmium sticking coefficient and δ is the sulfur sticking coefficient. In a similar manner α_2 can be calculated and shown to be a complex function of C_L . The influence of C_L as a function of C_L has not been calculated yet. These equations have been derived in the manner applied in reference (10). The nomenclature is the same as that appearing in the references.

2) The same type of an analysis can be carried out when it is assumed that the breaking up and recombining of atoms occurs at the kink site before their diffusion onto the crystal surface. In one case $2Cd$ and S_2 can be thought to leave the kink site simultaneously; or in the other case Cd can leave before the subsequent combination of sulfur into S_2 and the diffusion of S_2 and another Cd away from the kink site. These reactions can be expressed as follows:



The indices 1, 1', 3 and 4 denote the equilibrium or kink site (1), the activated state of the kink site (1'), the surface adsorption site (3) and the vapor phase (4). In this case two simultaneous processes occur; $1 \longrightarrow 3$ and $1 \longrightarrow 1' \longrightarrow 3$. When the rate determining steps are $1 \longrightarrow 3$ and $1 \longrightarrow 1'$, respectively, the following equation results:

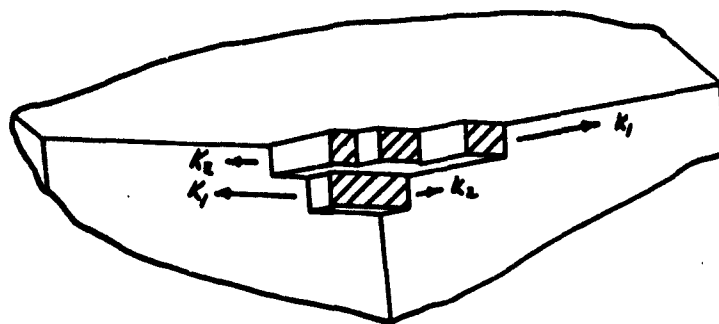
$$-\frac{dn}{Adt} = C_h \frac{k_{43}}{k_{34}} \left\{ 2k_{31} \frac{k_{43}}{k_{34}} \frac{k_{43}}{k_{34}} \left[(Cd_4^{23}S_4)_s - Cd_4^{2S}S_4 \right] + k_{1,1} \left[Cd_{4s} - Cd_4 \right] \right\} \quad (3)$$

The condensation coefficient α in this case would be a complex function of the various rates.

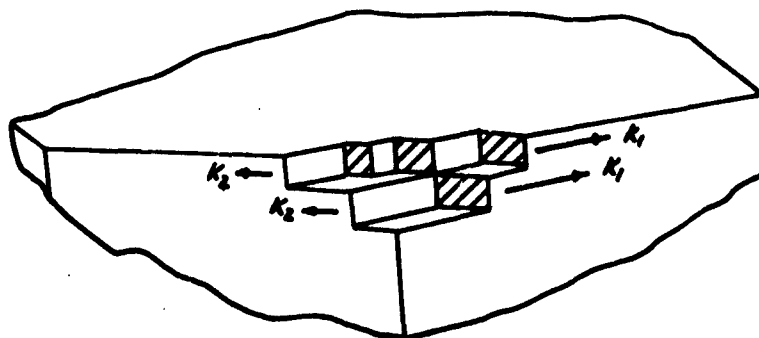
A great deal of attention should be placed on understanding the effects of crystal geometry on evaporation and condensation processes. These processes are a sensitive function of crystal geometry and important conclusions regarding surface reactions can be obtained when this effect is considered. As an example, the examination of the structures of wurtzite and sphalerite type materials indicates the existence of four different kinetic paths by which evaporation can occur. In wurtzite type materials two of these paths alternate for each succeeding basal plane layer. See Figure (9). In sphalerite type materials these paths are the same in each succeeding (111) layer but vary on different faces. This is also depicted in Figure (9). For wurtzite type materials the resulting evaporation form exhibits six-fold symmetry. For sphalerite type materials, however, the rapid evaporation rate is confined to three faces. As a result, a three-fold symmetry is observed on the evaporating form.

Mention should also be made of the role played by the structure on the rate of dissociation of a given material in various crystallographic directions. An F-plane will have the slowest dissociation rate. The rate of dissociation of any plane tilted with respect to two or more F-planes will depend on the dissociation rates of the F-planes involved. The rate will vary with the tilt angle and new F-planes will begin to influence this rate as the tilt angle is changed. These factors should be understood and accounted for in dissociation rate investigations since slow attack of a plane is often taken as a criterion for a high stability or a low chemical reactivity.

In conclusion, it is the determination of F-planes and the PBC vectors of these planes that are important in micromorphology studies. Important information on the bonding of surface atoms and the kinetics of growth and solution processes can be obtained from such studies.



(a)



(b)

Figure 9. - Schematic drawings of (a) wurtzite and (b) sphalerite type structures. K_1 and K_2 represent rate constants of an evaporation process; $K_1 \gg K_2$. For (a) the upper layer evaporates along bonding arrays in the direction indicated by the long arrow. The second layer, upon exposure, evaporates in the direction indicated by the long arrow for that layer. The process then repeats. Six-fold symmetry results. For (b) all the layers evaporate in the direction indicated by the long arrow. Three-fold symmetry results.

ACKNOWLEDGMENTS

Thanks are due to Messrs. J. D. Broder, J. J. Frawley and W. E. McCallum Jr. for their assistance in this work.

This paper was supported in part by the Air Force Research Division, Air Research and Development Command, United States Air Force under Contract AF33 (657)-7916, Contract AF33(657)-9975 and Contract AF33(616)-7528.

REFERENCES

- 1) G. A. Wolff, J. M. Wilbur Jr. and J. C. Clark, Z. Electrochem., 61, 101 (1957).
- 2) W. B. Pearson and G. A. Wolff, Faraday Society Discussions, 28, 112 (1959).
G. A. Wolff and J. G. Gualtieri, Am. Mineral., 47, 562 (1962).
G. A. Wolff, Z. Physik. Chem., 31, 1 (1962).
- 3) R. E. Schlier and H. E. Farnsworth, Semiconductor Surface Physics, Univ. of Pennsylvania Press (1951), p. 3.
H. E. Farnsworth, R. E. Schlier, T. H. George and R.M. Burger, J. Appl. Physics, 29, 1150 (1958).
- 4) N. W. Thibault, American Mineralogist, 29, 249 (1944).
- 5) G. A. Wolff and J. R. Hietanen, to be published.
- 6) a) N. W. Thibault, Am. Mineral., 29, 249 (1944).
b) L. S. Ramsdell and J. A. Kohn, Acta. Crystallogr., 5, 215 (1952).
c) L. S. Ramsdell and R. S. Mitchell, Am. Mineral., 38, 56 (1953).
d) N. W. Thibault, Am. Mineral., 33, 588 (1948).
- 7) J. G. Gualtieri, M. J. Katz and G. A. Wolff, Zeitschrift für Kristallographie, 111, 9 (1960).
- 8) G. A. Somorjai, This symposium.
G. A. Somorjai, Jour. Phys. Chem., 65, 1059 (1961).
- 9) A. Neuhaus and W. Retting, Zeit. Electrochemie, 62, 33 (1958).
- 10) I. N. Stranski and G. A. Wolff, Research, 4, 15 (1951).
O. Knacke, I. N. Stranski and G. A. Wolff, Z. Physik. Chem., 198, 157 (1951).